arXiv:1212.5413v1 [hep-ph] 21 Dec 2012

Anatomy of $B \to K\eta^{(\prime)}$ decays in different mixing schemes and effects of NLO contributions in the pQCD approach

Ying-Ying Fan, Wen-Fei Wang, Shan Cheng, and Zhen-Jun Xiao [a],

Department of Physics and Institute of Theoretical Physics,
Nanjing Normal University, Nanjing, Jiangsu 210023, P.R.China

(Dated: December 24, 2012)

Abstract

In this paper we make a comprehensive study about the four $B \to K\eta^{(\prime)}$ decays in the perturbative QCD (pQCD) factorization approach. We calculate the CP-averaged branching ratios and CP-violating asymmetries of $B \to K\eta^{(\prime)}$ decays in the ordinary η-$\eta^\prime$ mixing scheme, the η-$\eta^\prime$-G and the η-$\eta^\prime$-G-η_c mixing scheme, respectively. Besides the full leading order (LO) contributions, all currently known next-to-leading order (NLO) contributions to $B \to K\eta^{(\prime)}$ decays in the pQCD approach are taken into account. From our calculations and phenomenological analysis, we find that (a) the NLO contributions in general can provide significant enhancements to the LO pQCD predictions for the decay rates of the two $B \to K\eta^\prime$ decays, around $70\% - 89\%$ in magnitude, but result in relatively small changes to $Br(B \to K\eta)$; (b) although the NLO pQCD predictions in all three considered mixing schemes agree well with the data within one standard deviation, but those pQCD predictions in the η-$\eta^\prime$-G mixing scheme provide the best interpretation for the measured pattern of $Br(B \to K\eta^{(\prime)})$: $Br(B^0 \to K^0\eta) \approx 1.13 \times 10^{-6}$, $Br(B^0 \to K^0\eta^\prime) \approx 66.5 \times 10^{-6}$, $Br(B^\pm \to K^\pm\eta) \approx 2.36 \times 10^{-6}$, and $Br(B^\pm \to K^\pm\eta^\prime) \approx 67.3 \times 10^{-6}$, which agree perfectly with the measured values; (c) the NLO pQCD predictions for the CP-violating asymmetries for the four considered decays are also in good consistent with the data; (d) the newly known NLO contribution to the relevant form factors $\mathcal{M}_{FF}$ can produce about 20% enhancement to the branching ratios $Br(B \to K\eta^\prime)$, which plays an important role in closing the gap between the pQCD predictions and the relevant data; (e) the general expectations about the relative strength of the LO and NLO contributions from different sources are examined and confirmed by explicit numerical calculations.

PACS numbers: 13.25.Hw, 12.38.Bx, 14.40.Nd

---

[a] Electronic address: xiaozhenjun@njnu.edu.cn

I. INTRODUCTION

From the first observation of unexpectedly large branching ratios for $B \to K\eta'$ decays was reported by CLEO in 1997 [1], the four $B \to K\eta^{(\prime)}$ decays have been a "hot" topic for a long time. Although many physicists have made great efforts to explain the pattern of very large branching ratios $Br(B \to K\eta')$ and very small branching ratios $Br(B \to K\eta)$ [2–9], but it is still a hard job to understand such pattern in the framework of the standard model(SM).

On the experimental side, the branching ratios of the four $B \to K\eta^{(\prime)}$ decays have been measured with high precision [10, 11]:

$$\begin{aligned} Br(B^0 \to K^0\eta) &= (1.23^{+0.27}_{-0.24}) \times 10^{-6}, \\ Br(B^0 \to K^0\eta') &= (66.1 \pm 3.1) \times 10^{-6}, \\ Br(B^\pm \to K^\pm\eta) &= (2.36^{+0.22}_{-0.21}) \times 10^{-6}, \\ Br(B^\pm \to K^\pm\eta') &= (71.1 \pm 2.6) \times 10^{-6}, \end{aligned} \tag{1}$$

For the relevant CP-violating asymmetries, currently known experimental measurements are [10, 11]

$$\begin{aligned} \mathcal{A}_{CP}^{dir}(B^0 \to K^0\eta') &= (1 \pm 9)\%, \\ \mathcal{A}_{CP}^{mix}(B^0 \to K^0\eta') &= (64 \pm 11)\%, \\ \mathcal{A}_{CP}^{dir}(B^\pm \to K^\pm\eta) &= (-37 \pm 8)\%, \\ \mathcal{A}_{CP}^{dir}(B^\pm \to K^\pm\eta') &= (1.3^{+1.6}_{-1.7})\%, \end{aligned} \tag{2}$$

On the theory side, these decays are calculated recently in Ref. [12] by employing the perturbative QCD factorization approach[9] and using the ordinary Feldmann-Kroll-Stech (FKS) $\eta-\eta'$ mixing scheme [13], with the inclusion of the partial NLO contributions, i.e., the QCD vertex corrections, the quark-loops and the chromo-magnetic penguins O_{8g}. In Ref. [12] the authors found that the NLO contributions can provide a 70% enhancement to the LO pQCD predictions for $Br(B \to K\eta')$, but a 30% reduction to the LO pQCD predictions for $Br(B \to K\eta)$ [12]: numerically $Br(B^0 \to K^0\eta) \approx 2.1 \times 10^{-6}$, $Br(B^0 \to K^0\eta') \approx 50.3 \times 10^{-6}$, $Br(B^+ \to K^+\eta) \approx 3.2 \times 10^{-6}$, and $Br(B^\pm \to K^\pm\eta') \approx 51.0 \times 10^{-6}$; although the differences between the pQCD predictions and the data decreased effectively by the inclusion of the partial NLO contributions, but the central values of the pQCD predictions for $Br(B \to K\eta')$ are still lower than the data by about 30%. As for the CP-violating asymmetries, the pQCD predictions in Ref. [12] are basically agree well with the data.

Very recently, three new progresses in the studies of the two-body charmless hadronic $B \to M_2M_3$ decays (here M_i stands for the light mesons, such as $\pi, K, \eta^{(\prime)}, etc.$) in the pQCD approach have been made:

(i) In Ref. [14], Li et al. calculated the NLO contributions to the form factors of $B \to \pi$ transitions in the pQCD approach and found that the NLO part can provide about 20% enhancement to the LO one. The enhanced form factors may then lead to a larger branching ratio for $B \to K\eta'$ decays. The still missing NLO parts in the pQCD approach are the $O(\alpha_s^2)$ contributions from non-factorizable spectator diagrams and the annihilation diagrams, they are most possibly small according to general arguments.

(ii) In Ref. [15], the authors studied and provided a successful pQCD interpretation for the Belle measurements of $B_d/B_s \to J/\Psi\eta^{(\prime)}$, i.e., $R_q^{exp} = Br(B_q \to J/\Psi\eta')/Br(B_q \to J/\Psi\eta) < 1$ with $q = (d,s)$, by using the $\eta - \eta' - G$ mixing formalism[16], where G represents the pseudoscalar glueball. This result encourage us to check the possible effects of the pseudoscalar G on $B \to K\eta^{(\prime)}$ decays, although such contributions may be small as generally expected [17].

(iii) In Ref. [18], the authors studied the $\eta - \eta' - G - \eta_c$ mixing scheme, obtained constraints on the mixing angle ϕ_G, $\phi_G \sim 11^\circ$, between G and η_c by fitting to the observed η_c decay widths and other relevant data, and found that the η_c mixing can enhance the pQCD predictions for $Br(B \to K\eta')$ by 18%, but does not alter those for $Br(B \to K\eta)$. In Ref. [18], the authors superposed the contributions from $B \to K\eta_c$ due to the η_c mixing onto the partial pQCD predictions as given in Ref. [12] directly. They did not consider the effects of newly known NLO contributions to the corresponding form factors $F_0^{B\to K}(0)$ and $F_0^{B\to\eta^{(\prime)}}(0)$.

Motivated by above new progresses[14, 15, 18], we think that it is time for us to make a comprehensive study for the four $B \to K\eta^{(\prime)}$ decays in the pQCD factorization approach. We will focus on the following points:

(i) Besides those NLO contributions already considered in Ref. [12], we here will firstly extend the calculation of the NLO part of the form factors for $B \to \pi$ transition [14] to the cases for the similar $B \to K$ and $B \to (\eta_q, \eta_s)$ transitions, and then take these newly known form factors at NLO level into the calculations for the branching ratios and CP-violating asymmetries of $B \to K\eta^{(\prime)}$ decays, to check its effects on the corresponding pQCD predictions.

(ii) Besides the ordinary $\eta - \eta'$ mixing scheme [13], we will also calculate these four decays in the $\eta - \eta' - G$ [16] mixing scheme and the $\eta - \eta' - G - \eta_c$ mixing scheme [18], respectively. We want to check the effects of the possible "pseudoscalar Gluball" and η_c component of $\eta^{(\prime)}$ meson on the pQCD predictions.

(iii) We will calculate numerically for the individual decay amplitudes $\mathcal{M}^{a+b}$ (the emission diagrams Figs.1(a)-1(b)), $\mathcal{M}^{c+d}$ (the spectator diagrams Figs.1(c)-1(d)) and $\mathcal{M}^{anni}$ (annihilation diagrams Figs.1(e)-1(h)) and compare the relative strength of the contributions from different set of the Feynman diagrams at the leading order, or from the different sources at the next-to-leading order: such as $\mathcal{M}_{VC}$ (i.e. NLO vertex corrections Figs.3(a)-3(d)) and $\mathcal{M}_{ql}$ (i.e. NLO chromo-magnetic penguins Figs.3(g)-3(h)). We try to find the source of the dominant contribution, to evaluate the possible strength of the two still missing NLO contributions in the pQCD approach.

The paper is organized as follows. In Sec. II, we give a brief discussion for the pQCD factorization approach and the three different kinds of mixing schemes: η-η', η-η'-G, and η-η'-G-η_c mixing schemes. In Sec. III, we make the analytic calculations of the relevant Feynman diagrams and present the various decay amplitudes for the studied decay modes in leading-order. In Sec. IV, all currently known NLO contributions in the pQCD approach will be investigated. In Sec. V, we will show the numerical results for the pQCD predictions for the branching ratios and CP-violating asymmetries of the considered decay modes, we here also calculate and compare the relative strength of the LO and NLO contributions from different set of the Feynman diagrams or from different sources. The summary and some discussions are included in the final section.

II. THEORETICAL FRAMEWORK

As is well-known, the pQCD factorization approach has been widely used in studies for the two body charmless hadronic $B/B_s/B_c \to M_2 M_3$ decays (here M_i stands for the light pseudo-scalar meson P, the vector meson V, the scalar meson S, etc.) [5, 8, 9, 12, 14, 19–25]. Some pQCD predictions, for example the large CP-violating asymmetries $\mathcal{A}_{CP}^{dir}(B^0 \to \pi^+\pi^-) \approx (30 \pm 10)\%$ in Ref. [6] and large branching ratio $Br(B_s \to \pi^+\pi^-) \approx 5 \times 10^{-6}$ in Refs. [20, 26], have been confirmed by experiments[25]. We here focus on the study for the four $B \to K\eta^{(\prime)}$ decays. For more details of the formalism of the pQCD factorization approach itself, one can see for example Refs. [9, 12, 21, 27].

A. Outline of $B \to K\eta^{(\prime)}$ decays in the pQCD approach

In the B-rest frame, we assume that the light final state meson M_2 and M_3 is moving along the direction of $n = (1, 0, \mathbf{0}_T)$ and $v = (0, 1, \mathbf{0}_T)$, respectively. We use x_i to denote the momentum fraction of the anti-quark in each meson, $k_{i\perp}$ the corresponding transverse momentum. Using the light-cone coordinates the B meson momentum P_B and the two final state meson's momenta P_2 and P_3 (for M_2 and M_3 respectively) can be written as

$$P_B = \frac{M_B}{\sqrt{2}}(1, 1, \mathbf{0}_{\rm T}), \quad P_2 = \frac{M_B}{\sqrt{2}}(1 - r_3^2, r_2^2, \mathbf{0}_{\rm T}), \quad P_3 = \frac{M_B}{\sqrt{2}}(r_3^2, 1 - r_2^2, \mathbf{0}_{\rm T}), \tag{3}$$

where $r_i = m_i/M_B$ with m_i is the mass of meson M_i. If we choose

$$\begin{aligned} k_1 &= \frac{m_B}{\sqrt{2}}\left(x_1, 0, \mathbf{k}_{1\rm T}\right), \quad k_2 = \frac{m_B}{\sqrt{2}}\left(x_2(1 - r_3^2), x_2 r_2^2, \mathbf{k}_{2\rm T}\right), \\ k_3 &= \frac{m_B}{\sqrt{2}}\left(x_3 r_3^2, x_3(1 - r_2^2), \mathbf{k}_{3\rm T}\right). \end{aligned} \tag{4}$$

The integration over the small components k_1^-, k_2^-, and k_3^+ will lead to the decay amplitudes conceptually

$$\begin{aligned} \mathcal{A}(B \to M_2 M_3) \sim &\int dx_1 dx_2 dx_3 b_1 db_1 b_2 db_2 b_3 db_3 \\ &\cdot {\rm Tr}\left[C(t)\Phi_B(x_1, b_1)\Phi_{M_2}(x_2, b_2)\Phi_{M_3}(x_3, b_3)H(x_i, b_i, t)S_t(x_i)\, e^{-S(t)}\right], \end{aligned} \tag{5}$$

where b_i is the conjugate space coordinate of k_{iT}. In above equation, $C(t)$ is the Wilson coefficient evaluated at scale t, $\Phi_B(x_1, b_1)$ is the wave function of the B meson, $\Phi_{M_2}(x_2, b_2)$ and $\Phi_{M_3}(x_3, b_3)$ are the wave functions of the final state meson M_2 and M_3, the function $S_t(x_i)$ and $e^{-S(t)}$ are the Sudakov form factors which suppresses the soft dynamics effectively [9].

For the studied $B \to K\eta^{(\prime)}$ decays, the corresponding weak effective Hamiltonian can be written as [28]:

$$\mathcal{H}_{eff} = \frac{G_F}{\sqrt{2}} \left\{ V_{ub}V_{uq}^* \Big[C_1(\mu)O_1^u(\mu) + C_2(\mu)O_2^u(\mu) \Big] - V_{tb}V_{tq}^* \Big[\sum_{i=3}^{10} C_i(\mu)O_i(\mu) \Big] \right\} + \text{H.c.}, \tag{6}$$

where $q = d, s$, $G_F = 1.16639 \times 10^{-5} GeV^{-2}$ is the Fermi constant, O_i $(i = 1, ..., 10)$ are the local four-quark operators[28]. The Wilson coefficients C_i in Eq.6 and the corresponding renormalization group evolution matrix are known currently at LO and NLO level [28].

In this paper, we will calculate $B \to K\eta^{(\prime)}$ decays in the pQCD approach with the inclusion of all known NLO contributions, focus on the effects of the newly known NLO contributions to the form factors $F_0^{B\to K}(0)$ and $F_0^{B\to\eta^{(\prime)}}(0)$ [14].

B. Different Mixing Schemes

In order to check the effects of different mixing schemes we will calculate the $B \to K\eta^{(\prime)}$ decays in the following three different mixing schemes(MS):

(i) MS-1: The conventional FKS scheme [13] of $\eta - \eta'$ mixing in the quark-flavor basis: $\eta_q = (u\bar{u} + d\bar{d})/\sqrt{2}$ and $\eta_s = s\bar{s}$;

(ii) MS-2: The η-η'-G mixing scheme defined in Ref. [16];

(iii) MS-3: The η-η'-G-η_c mixing scheme defined in Ref. [18].

Firstly, in the conventional $\eta - \eta'$ mixing scheme, the physical η and η' can be written as

$$\begin{pmatrix} \eta \\ \eta' \end{pmatrix} = \begin{pmatrix} F_1(\phi)(u\bar{u} + d\bar{d}) + F_2(\phi)\, s\bar{s} \\ F_1'(\phi)(u\bar{u} + d\bar{d}) + F_2'(\phi)\, s\bar{s} \end{pmatrix} \tag{7}$$

where ϕ is the mixing angle, and

$$\begin{aligned} \sqrt{2}F_1(\phi) = F_2'(\phi) &= \cos(\phi), \\ F_2(\phi) = -\sqrt{2}F_1'(\phi) &= -\sin(\phi), \end{aligned} \tag{8}$$

are the mixing parameters. The relation between the decay constants $(f_\eta^q, f_\eta^s, f_{\eta'}^q, f_{\eta'}^s)$ and $(f_q, f_s,)$ can be found in Ref. [12]. The chiral enhancement m_0^q and m_0^s have been defined in Ref. [21] by assuming the exact isospin symmetry $m_q = m_u = m_d$. The three input parameters f_q, f_s and ϕ in the FKS mixing scheme have been extracted from the data of the relevant exclusive processes [13]:

$$f_q = (1.07 \pm 0.02)f_\pi, \quad f_s = (1.34 \pm 0.06)f_\pi, \quad \phi = 39.3^\circ \pm 1.0^\circ, \tag{9}$$

with $f_\pi = 0.13$ GeV.

In the η-η'-G mixing scheme [16], however, the physical states (η, η', G) are related to (η_q, η_s, g) through the rotation $U(\phi, \phi_G)$

$$\begin{pmatrix} |\eta\rangle \\ |\eta'\rangle \\ |G\rangle \end{pmatrix} = U(\phi, \phi_G) \begin{pmatrix} |\eta_q\rangle \\ |\eta_s\rangle \\ |g\rangle \end{pmatrix}, \tag{10}$$

with the rotation matrix

$$U(\phi,\phi_G)=\begin{pmatrix} \cos\phi+\sin\theta\sin\theta_i\Delta_G & -\sin\phi+\sin\theta\cos\theta_i\Delta_G & -\sin\theta\sin\phi_G \\ \sin\phi-\cos\theta\sin\theta_i\Delta_G & \cos\phi-\cos\theta\cos\theta_i\Delta_G & \cos\theta\sin\phi_G \\ -\sin\theta_i\sin\phi_G & -\cos\theta_i\sin\phi_G & \cos\phi_G \end{pmatrix}, \quad (11)$$

where $\Delta G = 1-\cos\phi_G$, $\theta_i = 54.7^\circ$ is the ideal mixing angle, $\phi=\theta+\theta_i$ with the θ varying in the range of $-17^\circ < \theta < -11^\circ$. Based on recent analysis[16, 18], we will choose

$$\theta=-11^\circ, \quad \phi_G = 12^\circ, \quad f_q = f_\pi, \quad f_s = 1.3 f_\pi, \quad m_G = 1.376\text{GeV}, \quad (12)$$

in the numerical calculations.

The decay constants associated with the physical (η, η', G) states are related to those associated with (η_q, η_s, g) states via the same mixing matrix

$$\begin{pmatrix} f_\eta^q & f_\eta^s \\ f_{\eta'}^q & f_{\eta'}^s \\ f_G^q & f_G^s \end{pmatrix} = U(\phi,\phi_G)\begin{pmatrix} f_q & f_q^s \\ f_s^q & f_s \\ f_g^q & f_g^s \end{pmatrix}. \quad (13)$$

Following Ref. [16], the chiral enhancement m_0^q and m_0^s in the η-η'-G mixing scheme can be written as

$$m_0^q = \frac{m_{qq}^2}{2m_q} = \frac{1}{2m_q}(U_{11} - \frac{\sqrt{2}f_s}{f_q}U_{12}), \quad (14)$$

$$m_0^s = \frac{m_{ss}^2}{2m_s} = \frac{1}{2m_s}(U_{22} - \frac{f_q}{\sqrt{2}f_s}U_{21}), \quad (15)$$

with

$$U_{11} = (\cos\phi+\sin\theta\sin\theta_i\Delta_G)^2 m_\eta^2 + (\sin\phi-\cos\theta\sin\theta_i\Delta_G)^2 m_{\eta'}^2 + (\sin\theta_i\sin\phi_G)^2 m_G^2, \quad (16)$$

$$\begin{aligned} U_{12} = U_{21} &= (\cos\phi+\sin\theta\sin\theta_i\Delta_G)\cdot(-\sin\phi+\sin\theta\cos\theta_i\Delta_G)m_\eta^2 \\ &+(\sin\phi-\cos\theta\sin\theta_i\Delta_G)\cdot(\cos\phi-\cos\theta\cos\theta_i\Delta_G)m_{\eta'}^2 \\ &+\sin\theta_i\sin\phi_G\cdot\cos\theta_i\sin\phi_G m_G^2\ , \quad (17) \end{aligned}$$

$$\begin{aligned} U_{22} &= (-\sin\phi+\sin\theta\cos\theta_i\Delta_G)^2 m_\eta^2 + (\cos\phi-\cos\theta\cos\theta_i\Delta_G)^2 m_{\eta'}^2 \\ &+(\cos\theta_i\sin\phi_G)^2 m_G^2\ . \quad (18) \end{aligned}$$

In the third η-η'-G-η_c mixing scheme, finally, the flavor states are transformed into the physical states through the mixing matrix $U(\theta,\phi_G,\phi_Q)$:

$$\begin{pmatrix} |\eta\rangle \\ |\eta'\rangle \\ |G\rangle \\ |\eta_c\rangle \end{pmatrix} = U(\theta,\phi_G,\phi_Q)\begin{pmatrix} |\eta_q\rangle \\ |\eta_s\rangle \\ |g\rangle \\ |\eta_Q\rangle \end{pmatrix}, \quad (19)$$

with the 4×4 mixing matrix

$$U(\theta,\phi_G,\phi_Q)=\begin{pmatrix} c\theta c\theta_i - s\theta c\phi_G s\theta_i & -c\theta s\theta_i - s\theta c\phi_G c\theta_i & -s\theta s\phi_G c\phi_Q & -s\theta s\phi_G s\phi_Q \\ s\theta c\theta_i + c\theta c\phi_G s\theta_i & -s\theta s\theta_i + c\theta c\phi_G c\theta_i & c\theta s\phi_G c\phi_Q & c\theta s\phi_G s\phi_Q \\ -s\phi_G s\theta_i & -s\phi_G c\theta_i & c\phi_G c\phi_Q & c\phi_G s\phi_Q \\ 0 & 0 & -s\phi_Q & c\phi_Q \end{pmatrix} \quad (20)$$

where $c\phi$ ($s\phi$) is the shorthand notation for $\cos\phi$ ($\sin\phi$) and similarly for others. The decay constants associated with the η, η', G, and η_c physical states are related to those associated with the η_q, η_s, g, η_Q states through the mixing matrix $U(\theta, \phi_G, \phi_Q)$:

$$\begin{pmatrix} f^q_\eta & f^s_\eta & f^c_\eta \\ f^q_{\eta'} & f^s_{\eta'} & f^c_{\eta'} \\ f^q_G & f^s_G & f^c_G \\ f^q_{\eta_c} & f^s_{\eta_c} & f^c_{\eta_c} \end{pmatrix} = U(\theta, \phi_G, \phi_Q) \begin{pmatrix} f_q & f^s_q & f^c_q \\ f^q_s & f_s & f^c_s \\ f^q_g & f^s_g & f^c_g \\ f^q_c & f^s_c & f_c \end{pmatrix}. \tag{21}$$

Furthermore, we find that the chiral enhancement m_0^q and m_0^s in the third mixing scheme are identical to those as given in Eqs. (14,15). In η-η'-G-η_c mixing scheme, we take $\phi_Q = 11^\circ$ and choose the same input parameters $(\theta, \phi_G, f_q, f_s, m_G)$ as given in Eq.(12).

C. Wave Functions

The B meson is treated as a very good heavy-light system. Its wave function can be written as the form of

$$\Phi_B = \frac{i}{\sqrt{2N_c}}(\not{P}_B + m_B)\gamma_5 \phi_B(\mathbf{k_1}). \tag{22}$$

Here we adopted the widely used B-meson distribution amplitude in the pQCD approach

$$\phi_B(x,b) = N_B x^2(1-x)^2 \mathrm{exp}\left[-\frac{M_B^2\ x^2}{2\omega_b^2} - \frac{1}{2}(\omega_b b)^2\right], \tag{23}$$

where the normalization factor N_B depends on the value of ω_b and f_B and defined through the normalization relation

$$\int_0^1 dx\ \phi_B(x, b=0) = \frac{f_B}{2\sqrt{6}}. \tag{24}$$

For the shape parameter ω_b we take $\omega_b = 0.4 \pm 0.04$ GeV in numerical calculations.

The wave functions of the final state mesons $M = (K, \eta_q, \eta_s)$ are defined as:

$$\Phi_{M_i}(P_i, x_i) \equiv \frac{i}{\sqrt{2N_C}}\gamma_5\left[\not{P}_2\phi^A_{M_i}(x_i) + m_{0i}\phi^P_{M_i}(x_i) - m_{0i}(\not{n}\not{v} - 1)\phi^T_{M_i}(x_i)\right], \tag{25}$$

where m_{0i} is the corresponding meson chiral mass, P_i and x_i are the momentum and the momentum fraction of M_i, respectively. The explicit expressions of the distribution amplitudes $\phi^{A,P,T}_{M_i}(x_i)$ for $M = (K, \eta_q, \eta_s)$ will be given at Appendix A.

In the third η-η'-G-η_c mixing scheme, the η_c part of the $\eta^{(\prime)}$ meson will contribute to the $B \to K\eta^{(\prime)}$ decays through the decay chain $B \to K\eta_c \to K\eta^{(\prime)}$. The wave function of the η_c can be written as[29]:

$$\Phi_{\eta_c}(P_2, x_2) \equiv \frac{i}{\sqrt{2N_C}}\gamma_5[\not{P}_2\phi^\nu_{\eta_c}(x_2) + m_{\eta_c}\phi^s_{\eta_c}(x_2)]. \tag{26}$$

The distribution amplitudes $\phi^{\nu,s}_{\eta_c}$ are of the form [29]:

$$\begin{aligned} \phi^\nu_{\eta_c}(x) &= 9.58\frac{f_{\eta_c}}{2\sqrt{2N_c}}x(1-x)\Big[\frac{x(1-x)}{1-2.8x(1-x)}\Big]^{0.7}, \\ \phi^s_{\eta_c}(x) &= 1.97\frac{f_{\eta_c}}{2\sqrt{2N_c}}\Big[\frac{x(1-x)}{1-2.8x(1-x)}\Big]^{0.7}. \end{aligned} \tag{27}$$

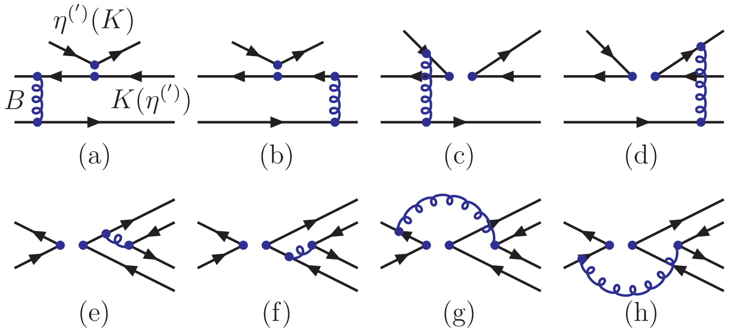

FIG. 1. Feynman diagrams which may contribute to the $B \to K\eta^{(\prime)}$ decays in the pQCD approach at leading order.

III. $B \to K\eta^{(\prime)}$ AND $B \to K\eta_c$ DECAYS AT LEADING ORDER

In this section we will present the total decay amplitudes for $B \to K\eta^{(\prime)}$ and $B \to K\eta_c$ decays in the pQCD approach at leading order.

A. $B \to K\eta^{(\prime)}$ decays at leading order

The $B \to K\eta^{(\prime)}$ decays have been studied by using the ordinary η-η' mixing scheme and by employing the pQCD factorization approach at the LO and partial NLO level in Ref. [12]. We recalculated and confirmed the relevant analytical formulas as given in Ref. [12]. For the sake of the reader, we here present directly the decay amplitudes obtained by evaluating the Feynman diagrams Fig.1(a)-1(h).

For the factorizable emission diagrams Figs.1(a)-1(b), the decay amplitudes for the cases of $B \to K$ transition are of the form:

$$\begin{aligned} F_{eK}^{V-A} = -F_{eK}^{V+A} = &-8\pi C_F M_B^4 \int_0^1 dx_1 dx_3 \int_0^\infty b_1 db_1 b_3 db_3 \phi_B(x_1,b_1) \\ &\times\Big\{ \Big[(1+x_3)\phi_K^A(x_3) + r_3(1-2x_3)(\phi_K^P(x_3)+\phi_K^T(x_3))\Big] \\ &\times E_e(t_a) h_e(x_1,x_3,b_1,b_3) + 2r_3\phi_K^P(x_3)E_e(t_a')h_e(x_3,x_1,b_3,b_1)\Big\}, \end{aligned} \quad (28)$$

$$\begin{aligned} F_{eK}^{SP} = &-16\pi r_2 C_F M_B^4 \int_0^1 dx_1 dx_3 \int_0^\infty b_1 db_1 b_3 db_3 \phi_B(x_1,b_1) \\ &\times\Big\{ \Big[\phi_K^A(x_3) + r_3(2+x_3)\phi_K^P(x_3) - r_3 x_3 \phi_K^T(x_3)\Big] \\ &\times E_e(t_a) h_e(x_1,x_3,b_1,b_3) + 2r_3\phi_K^P(x_3)E_e(t_a')h_e(x_3,x_1,b_3,b_1)\Big\}, \end{aligned} \quad (29)$$

where $C_F = 4/3$, $r_2 = r_\eta = m_0^{q,s}/M_B$ and $r_3 = r_K = m_0^K/M_B$, where $m_0^{q,s}$ and m_0^K are the chiral scale parameters. The functions $E_e(t)$, the definitions of the factorization scales t and the hard functions h_e are given in Appendix B.

For the non-factorizable emission diagrams Figs.1(c)-1(d), whose contributions are

$$
\begin{aligned}
M_{eK}^{V-A} = & -32\pi C_F M_B^4/\sqrt{6}\int_0^1 dx_1dx_2dx_3\int_0^\infty b_1db_1b_2db_2\phi_B(x_1,b_1)\phi_\eta^A(x_2) \\
& \times\Big\{\Big[(1-x_2)\phi_K^A(x_3)-r_3x_3(\phi_K^P(x_3)-\phi_K^T(x_3))\Big]E_e'(t_b)h_n(x_1,\bar{x}_2,x_3,b_1,b_2) \\
& +\Big[-(x_2+x_3)\phi_K^A(x_3)+r_3x_3(\phi_K^P(x_3)+\phi_K^T(x_3))\Big] \\
& \times E_e'(t_b')h_n(x_1,x_2,x_3,b_1,b_2)\Big\}, \qquad (30)
\end{aligned}
$$

$$
\begin{aligned}
M_{eK}^{V+A} = & -32\pi C_F M_B^4 r_2/\sqrt{6}\int_0^1 dx_1dx_2dx_3\int_0^\infty b_1db_1b_2db_2\phi_B(x_1,b_1) \\
& \times\Big\{\Big[(1-x_2)\phi_K^A(x_3)\left(\phi_\eta^P(x_2)+\phi_\eta^T(x_2)\right) \\
& +r_3x_3\left(\phi_\eta^P(x_2)-\phi_\eta^T(x_2)\right)\left(\phi_K^P(x_3)+\phi_K^T(x_3)\right) \\
& +(1-x_2)r_3\left(\phi_2^P(x_2)+\phi_2^T(x_2)\right)\left(\phi_3^P(x_3)-\phi_3^T(x_3)\right)\Big]E_e'(t_b)h_n(x_1,\bar{x}_2,x_3,b_1,b_2) \\
& -\Big[x_2\phi_K^A(x_3)(\phi_\eta^P(x_2)-\phi_\eta^T(x_2))+r_3x_2(\phi_\eta^P(x_2)-\phi_\eta^T(x_2)) \\
& (\phi_K^P(x_3)-\phi_K^T(x_3))+r_3x_3(\phi_\eta^P(x_2)+\phi_\eta^T(x_2))(\phi_K^P(x_3)+\phi_K^T(x_3))\Big] \\
& \times E_e'(t_b')h_n(x_1,x_2,x_3,b_1,b_2)\Big\}, \qquad (31)
\end{aligned}
$$

$$
\begin{aligned}
M_{eK}^{SP} = & -32\pi C_F M_B^4/\sqrt{6}\int_0^1 dx_1dx_2dx_3\int_0^\infty b_1db_1b_2db_2\phi_B(x_1,b_1)\phi_\eta^A(x_2) \\
& \times\Big\{\Big[(x_2-x_3-1)\phi_K^A(x_3)+r_3x_3(\phi_K^P(x_3)+\phi_K^T(x_3))\Big]E_e'(t_b)h_n(x_1,\bar{x}_2,x_3,b_1,b_2) \\
& +\Big[x_2\phi_K^A(x_3)+r_3x_3(\phi_K^T(x_3)-\phi_K^P(x_3))\Big]E_e'(t_b')h_n(x_1,x_2,x_3,b_1,b_2)\Big\}, \qquad (32)
\end{aligned}
$$

where $\bar{x}_i = 1-x_i$, while ϕ_η denotes ϕ_{η_q} or ϕ_{η_s}.

For the factorizable annihilation diagrams Fig.1(e)-1(f), the decay amplitudes are of the form

$$
\begin{aligned}
F_{aK}^{V-A} = F_{aK}^{V+A} = & -8\pi C_F M_B^4\int_0^1 dx_2dx_3\int_0^\infty b_2db_2b_3db_3 \\
& \times\Big\{\Big[(x_3-1)\phi_\eta^A(x_2)\phi_K^A(x_3)-4r_2r_3\phi_\eta^P(x_2)\phi_K^P(x_3) \\
& +2r_2r_3x_3\phi_\eta^P(x_2)(\phi_K^P(x_3)-\phi_K^T(x_3))\Big]E_a(t_c)h_a(x_2,\bar{x}_3,b_2,b_3) \\
& +\Big[x_2\phi_\eta^A(x_2)\phi_K^A(x_3)+2r_2r_3(\phi_\eta^P(x_2)-\phi_\eta^T(x_2))\phi_K^P(x_3) \\
& +2r_2r_3x_2(\phi_\eta^P(x_2)+\phi_\eta^T(x_2))\phi_K^P(x_3)\Big]E_a(t_c')h_a(\bar{x}_3,x_2,b_3,b_2)\Big\}. \qquad (33)
\end{aligned}
$$

$$
\begin{aligned}
F_{aK}^{SP} = & -16\pi C_F M_B^4\int_0^1 dx_2dx_3\int_0^\infty b_2db_2b_3db_3 \\
& \times\Big\{\Big[2r_2\phi_\eta^P(x_2)\phi_K^A(x_3)+(1-x_3)r_3\phi_\eta^A(x_2)(\phi_K^P(x_3)+\phi_K^T(x_3))\Big]E_a(t_c)h_a(x_2,\bar{x}_3,b_2,b_3) \\
& +\Big[2r_3\phi_\eta^A(x_2)\phi_K^P(x_3)+r_2x_2(\phi_\eta^P(x_2)-\phi_\eta^T(x_2))\phi_K^A(x_3)\Big]E_a(t_c')h_a(\bar{x}_3,x_2,b_3,b_2)\Big\}. \qquad (34)
\end{aligned}
$$

For the non-factorizable annihilation diagrams Figs.1(g)-1(h), whose contributions are

$$
\begin{aligned}
M_{aK}^{V-A} = & -32\pi C_F M_B^4/\sqrt{6}\int_0^1 dx_1 dx_2 dx_3 \int_0^\infty b_1 db_2 b_2 db_2 \phi_{B_s}(x_1,b_1) \\
& \times\Big\{\Big[- x_2\phi_\eta^A(x_2)\phi_K^A(x_3) - 4r_2r_3\phi_\eta^P(x_2)\phi_K^P(x_3) \\
& + r_2r_3(1-x_2)(\phi_\eta^P(x_2)+\phi_\eta^T(x_2))(\phi_K^P(x_3)-\phi_K^T(x_3)) \\
& + r_2r_3x_3(\phi_\eta^P(x_2)-\phi_\eta^T(x_2))(\phi_K^P(x_3)+\phi_K^T(x_3))\Big] E_a'(t_c) h_{na}(x_1,x_2,x_3,b_1,b_2) \\
& + \Big[\bar{x}_3\phi_\eta^A(x_2)\phi_K^A(x_3) + \bar{x}_3 r_2r_3(\phi_\eta^P(x_2)+\phi_\eta^T(x_2))(\phi_K^P(x_3)-\phi_K^T(x_3)) \\
& + x_2r_2r_3(\phi_\eta^P(x_2)-\phi_\eta^T(x_2))(\phi_K^P(x_3)+\phi_K^T(x_3))\Big] \\
& \times E_a'(t_c') h_{na}'(x_1,x_2,x_3,b_1,b_2)\Big\}, \qquad (35)
\end{aligned}
$$

$$
\begin{aligned}
M_{aK}^{V+A} = & -32\pi C_F M_{B_s}^4/\sqrt{6}\int_0^1 dx_1 dx_2 dx_3 \int^\infty b_1 db_1 b_2 db_2 \phi_B(x_1,b_1) \\
& \times\Big\{\Big[r_2(2-x_2)(\phi_\eta^P(x_2)+\phi_e ta^T(x_2))\phi_K^A(x_3) \\
& - r_3(1+x_3)\phi_\eta^A(x_2)(\phi_K^P(x_3)-\phi_K^T(x_3))\Big] E_a'(t_d) h_{na}(x_1,x_2,x_3,b_1,b_2) \\
& + \Big[r_2x_2\left(\phi_\eta^P(x_2)+\phi_\eta^T(x_2)\right)\phi_K^A(x_3) - r_3\bar{x}_3\phi_\eta^A(x_2)(\phi_K^P(x_3)-\phi_K^T(x_3))\Big] \\
& \times E_a'(t_d') h_{na}'(x_1,x_2,x_3,b_1,b_2)\Big\}. \qquad (36)
\end{aligned}
$$

$$
\begin{aligned}
M_{aK}^{SP} = & -32\pi C_F M_B^4/\sqrt{6}\int_0^1 dx_1 dx_2 dx_3 \int_0^\infty b_1 db_1 b_2 db_2 \phi_B(x_1,b_1) \\
& \times\Big\{\Big[(x_3-1)\phi_\eta^A(x_2)\phi_K^A(x_3) - 4r_2r_3\phi_\eta^P(x_2)\phi_K^P(x_3) \\
& + r_2r_3x_3(\phi_\eta^P(x_2)+\phi_\eta^T(x_2))(\phi_K^P(x_3)-\phi_K^T(x_3)) \\
& + r_2r_3(1-x_2)(\phi_\eta^P(x_2)-\phi_\eta^T(x_2))(\phi_K^P(x_3)+\phi_K^T(x_3))\Big] \\
& \times E_a'(t_d) h_{na}(x_1,x_2,x_3,b_1,b_2) \\
& + \Big[x_2\phi_\eta^A(x_2)\phi_K^A(x_3) + x_2r_2r_3(\phi_\eta^P(x_2)+\phi_\eta^T(x_2))(\phi_K^P(x_3)-\phi_K^T(x_3)) \\
& + r_2r_3(1-x_3)(\phi_\eta^P(x_2)-\phi_\eta^T(x_2))(\phi_K^P(x_3)+\phi_K^T(x_3))\Big] \\
& \times E_a'(t_d') h_{na}'(x_1,x_2,x_3,b_1,b_2)\Big\}. \qquad (37)
\end{aligned}
$$

The evolution functions $E_i(t)$ and hard functions h_i appeared in Eqs. (28-37) are given explicitly in Appendix B.

If we exchange the position of K and $\eta^{(\prime)}$ in Fig. 1, we will find the corresponding decay amplitudes for the case of $B \to \eta^{(\prime)}$ transitions. Since the K and $\eta^{(\prime)}$ are all pseudoscalar mesons and have the similar wave functions, the decay amplitudes for new diagrams, say $F_{e\eta}^{V-A}$, $F_{e\eta}^{V+A}$, $F_{e\eta}^{SP}$, $M_{e\eta}^{V-A}$, $M_{e\eta}^{V+A}$, $M_{e\eta}^{SP}$, $F_{a\eta}^{V-A}$, $F_{a\eta}^{V+A}$, $F_{a\eta}^{SP}$, $M_{a\eta}^{V-A}$, $M_{a\eta}^{V+A}$, and $M_{a\eta}^{SP}$ can be obtained from those as given in Eqs. (28-37) by the following replacements

$$
\phi_K^A \leftrightarrow \phi_{\eta^{(\prime)}}^A, \quad \phi_K^P \leftrightarrow \phi_{\eta^{(\prime)}}^P, \quad \phi_K^T \leftrightarrow \phi_{\eta^{(\prime)}}^T, \quad r_\eta \leftrightarrow r_K. \qquad (38)
$$

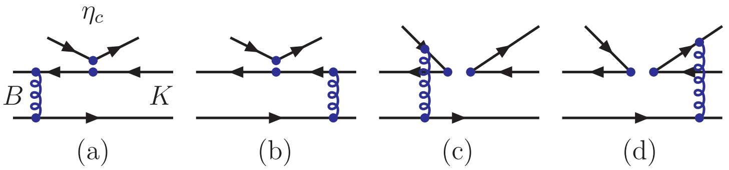

(a) (b) (c) (d)

FIG. 2. Feynman diagrams which may contribute to the $B \to K\eta_c$ decays in pQCD approach at leading order.

B. $B \to K\eta_c$ at leading order

For $B \to K\eta_c$ decays at leading order pQCD approach, the Feynman diagrams which may contribute are shown in Fig. 2. The $B \to K\eta_c$ decays have been studied in Ref. [23] in the pQCD approach, at the full leading order and with the inclusion of the partial NLO vertex corrections. We here recalculated theses decays and confirmed the results of Ref. [23]. The relevant decay amplitudes are the following

$$\begin{aligned}
F_{\eta_c K} &= 8\pi C_F M_B^2 \int_0^1 dx_1 dx_3 \int_0^\infty b_1 db_1 b_3 db_3 \phi_B(x_1,b_1) \\
&\quad \times \Big\{ \Big[[(1-r_{\eta_c}^2)(1+x_3) - x_3 r_{\eta_c}^2]\phi_K^A(x_3) + r_3(1-2x_3)[\phi_K^P(x_3)+\phi_K^T(x_3)] \\
&\quad + r_3 r_{\eta_c}^2 [(1+2x_3)\phi_K^P(x_3) - (1-2x_3)\phi_K^T(x_3)] \Big] E_e(t_e) h'_e(x_1,x_3,b_1,b_3) \\
&\quad + 2r_3(1-r_{\eta_c}^2)\phi_K^P(x_3) E_e(t'_e) h'_e(x_3,x_1,b_3,b_1) \Big\}, \qquad (39) \\
M_{\eta_c K} &= -\frac{32}{\sqrt{6}}\pi C_F M_B^2 \int_0^1 dx_1 dx_2 dx_3 \int_0^\infty b_1 db_1 b_2 db_2 \phi_B(x_1,b_1)\phi_{\eta_c}^{\nu}(x_2) \\
&\quad \times \Big[x_3(1-2r_{\eta_c}^2)\phi_K^A(x_3) - 2x_3 r_3(1-r_{\eta_c}^2)\phi_K^T(x_3) \Big] \\
&\quad \cdot E'_e(t'_f) h'_n(x_1,x_2,x_3,b_1,b_2), \qquad (40)
\end{aligned}$$

where $r_3 = m_0^K/m_B$, $r_{\eta_c} = m_{\eta_c}/m_B$, $r_c = m_c/m_B$. $\phi_{\eta_c}^{\nu}$ is the leading twist-2 part of the distribution amplitude for the pseudo-scalar meson η_c. The evolution function $E^{(\prime)}(t)$, hard function h_i and the scale t_e, t'_e will be given in Appendix B.

At the leading order pQCD approach, the total decay amplitude for $B \to \eta_c K$ decay can then be written as:

$$\begin{aligned}
\mathcal{M}(B \to \eta_c K) &= F_{\eta_c K} f_{\eta_c} \Big[V_{cb}^* V_{cs} a_2 - V_{tb}^* V_{ts}(a_3 - a_5 - a_7 + a_9) \Big] \\
&\quad + M_{\eta_c K} \Big[V_{cb}^* V_{cs} C_2 - V_{tb}^* V_{ts}(C_4 + C_6 + C_8 + C_{10}) \Big]. \qquad (41)
\end{aligned}$$

C. The total decays amplitudes of $B \to K\eta^{(\prime)}$ decays

For $B^0 \to K^0\eta$ and $B^+ \to K^+\eta$ decays, by combining the contributions from all possible Feynman diagrams Fig. 1 and Fig. 2, one finds the general expressions of the total decay amplitudes (here the Wilson coefficients and CKM factors are all included):

$$
\begin{aligned}
\mathcal{M}(K^0\eta) = \frac{G_F}{\sqrt{2}}\Big\{&\lambda_u\Big[a_2 f_\eta^q F_{eK}^{V-A} + C_2 M_{eK}^{V-A,q} F_1(\phi)\Big] - \lambda_t\left(2a_3 - 2a_5 - \frac{1}{2}a_7 + \frac{1}{2}a_9\right) f_\eta^q F_{eK}^{V-A} \\
&-\lambda_t\Big[\left(a_3 + a_4 - a_5 + \frac{1}{2}a_7 - \frac{1}{2}a_9 - \frac{1}{2}a_{10}\right) f_\eta^s F_{eK}^{V-A} \\
&+\left(a_6 - \frac{1}{2}a_8\right)\left[f_\eta^s F_{eK}^{SP} + f_B F_{aK}^{SP} F_2(\phi) + f_B F_{a\eta}^{SP} F_1(\phi) + f_K F_{e\eta}^{SP} F_1(\phi)\right] \\
&+\left(C_3 + C_4 - \frac{1}{2}C_9 - \frac{1}{2}C_{10}\right) M_{eK}^{V-A,s} F_2(\phi) \\
&+\left(2C_4 + \frac{1}{2}C_{10}\right) M_{eK}^{V-A,q} F_1(\phi) + \left(C_5 - \frac{1}{2}C_7\right) M_{eK}^{V+A,s} F_2(\phi) \\
&+\left(2C_6 + \frac{1}{2}C_8\right) M_{eK}^{SP,q} F_1(\phi) + \left(C_6 - \frac{1}{2}C_8\right) M_{eK}^{SP,s} F_2(\phi) \\
&+\left(a_4 - \frac{1}{2}a_{10}\right)\left[f_B F_{aK}^{V-A} F_2(\phi) + f_K F_{e\eta}^{V-A} F_1(\phi) + f_B F_{a\eta}^{V-A} F_1(\phi)\right] \\
&+\left(C_3 - \frac{1}{2}C_9\right)\left[M_{aK}^{V-A} F_2(\phi) + M_{e\eta}^{V-A} F_1(\phi) + M_{a\eta}^{V-A} F_1(\phi)\right] \\
&+\left(C_5 - \frac{1}{2}C_7\right)\left[M_{aK}^{V+A} F_2(\phi) + M_{e\eta}^{V+A} F_1(\phi) + M_{a\eta}^{V+A} F_1(\phi)\right]\Big]\Big\} \\
&+\mathcal{M}(B \to \eta_c K) * F_c(\theta, \phi_G, \phi_Q),
\end{aligned} \tag{42}
$$

$$
\begin{aligned}
\mathcal{M}(K^+\eta) = \frac{G_F}{\sqrt{2}}\Big\{&\lambda_u\Big[a_2 f_\eta^q F_{eK}^{V-A} + C_2 M_{eK}^{V-A,q} F_1(\phi) + a_1 f_B\left[F_{aK}^{V-A} F_2(\phi) + F_{a\eta}^{V-A} F_1(\phi)\right] \\
&+a_1 f_K F_{e\eta}^{V-A} F_1(\phi) + C_1\left[M_{aK}^{V-A} F_2(\phi) + M_{e\eta}^{V-A} F_1(\phi) + M_{a\eta}^{V-A} F_1(\phi)\right]\Big] \\
&-\lambda_t\Big[\left(2a_3 - 2a_5 - \frac{1}{2}a_7 + \frac{1}{2}a_9\right) f_\eta^q F_{eK}^{V-A} \\
&+\left(a_3 + a_4 - a_5 + \frac{1}{2}a_7 - \frac{1}{2}a_9 - \frac{1}{2}a_{10}\right) f_\eta^s F_{eK}^{V-A} \\
&+\left(a_6 - \frac{1}{2}a_8\right) f_\eta^s F_{eK}^{SP} + \left(C_3 + C_4 - \frac{1}{2}C_9 - \frac{1}{2}C_{10}\right) M_{eK}^{V-A,s} F_2(\phi) \\
&+\left(2C_4 + \frac{1}{2}C_{10}\right) M_{eK}^{V-A,q} F_1(\phi) + \left(C_5 - \frac{1}{2}C_7\right) M_{eK}^{V+A,s} F_2(\phi) \\
&+\left(2C_6 + \frac{1}{2}C_8\right) M_{eK}^{SP,q} F_1(\phi) + \left(C_6 - \frac{1}{2}C_8\right) M_{eK}^{SP,s} F_2(\phi) \\
&+(a_4 + a_{10})\left[f_B F_{aK}^{V-A} F_2(\phi) + f_K F_{e\eta}^{V-A} F_1(\phi) + f_B F_{a\eta}^{V-A} F_1(\phi)\right] \\
&+(a_6 + a_8)\left[f_B F_{aK}^{SP} F_2(\phi) + f_K F_{e\eta}^{SP} F_1(\phi) + f_B F_{a\eta}^{SP} F_1(\phi)\right] \\
&+(C_3 + C_9)\left[M_{aK}^{V-A} F_2(\phi) + M_{e\eta}^{V-A} F_1(\phi) + M_{a\eta}^{V-A} F_1(\phi)\right] \\
&+(C_5 + C_7)\left[M_{aK}^{V+A} F_2(\phi) + M_{e\eta}^{V+A} F_1(\phi) + M_{a\eta}^{V+A} F_1(\phi)\right]\Big]\Big\} \\
&+\mathcal{M}(B \to \eta_c K) * F_c(\theta, \phi_G, \phi_Q),
\end{aligned} \tag{43}
$$

where $\lambda_u = V_{ub}^* V_{us}$, $\lambda_t = V_{tb}^* V_{ts}$, while the Wilson coefficients a_i are defined as the combination of Wilson coefficients C_i through the following relations:

$$
\begin{aligned}
a_{1,2} &= C_{2,1} + \frac{C_{1,2}}{3}; \quad a_i = C_i + \frac{C_{i+1}}{3}, \quad for \quad i = 3,5,7,9; \\
a_i &= C_i + \frac{C_{i-1}}{3}, \quad for \quad i = 4,6,8,10.
\end{aligned} \tag{44}
$$

The expressions of the mixing parameters $F_i^{(')}(\phi)$ depend on the choice of the different mixing schemes:

(i) In MS-1, i.e. the FKS η-η' mixing scheme, $F_{1,2}(\phi)$ and $F'_{1,2}(\phi)$ have been defined in Eq. (8).

(ii) In MS-2, i.e. the η-η'-G mixing scheme, $F_{1,2}(\phi)$ and $F'_{1,2}(\phi)$ are of the form

$$
\begin{aligned}
F_1(\phi) &= \frac{1}{\sqrt{2}}(\cos\phi + \sin\theta \sin\theta_i \Delta_G), \quad F_2(\phi) = -\sin\phi + \sin\theta\cos\theta_i\Delta_G, \\
F'_1(\phi) &= \frac{1}{\sqrt{2}}(\sin\phi - \cos\theta \sin\theta_i \Delta_G), \quad F'_2(\phi) = \cos\phi - \cos\theta\cos\theta_i\Delta_G.
\end{aligned} \tag{45}
$$

(iii) In MS-3, i.e. the third η-η'-G-η_c mixing scheme, $F_{1,2}(\phi)$ and $F'_{1,2}(\phi)$ are are the same as given in Eq. (45). For this case, the η_c also contribute through mixing, and the relevant mixing parameters are

$$
F_c(\theta,\phi_G,\phi_Q) = -\sin\theta\sin\phi_G\sin\phi_Q, \quad F'_c(\theta,\phi_G,\phi_Q) = \cos\theta\sin\phi_G\sin\phi_Q. \tag{46}
$$

Finally, the total decay amplitudes for $B^0 \to K^0\eta'$ and $B^+ \to K^+\eta'$ in the pQCD approach at leading order can be obtained easily from Eqs. (42) and (43) by the following replacements

$$
\begin{aligned}
& f_\eta^q \to f_{\eta'}^q, \quad f_\eta^s \to f_{\eta'}^s, \\
& F_1(\phi) \to F'_1(\phi), \quad F_2(\phi) \to F'_2(\phi), \quad F_c(\phi) \to F'_c(\phi).
\end{aligned} \tag{47}
$$

IV. NLO CONTRIBUTIONS IN THE PQCD APPROACH

As is well-known, the power counting rule in the pQCD factorization approach [21] is rather different from that in the QCD factorization[7, 30, 31]. When compared with the previous LO calculations in pQCD [9], the full pQCD predictions should include the following NLO contributions:

(1) We should use the Wilson coefficients $C_i(m_W)$ at NLO level in the NDR scheme [28], the NLO renormalization group (RG) evolution matrix $U(t, m, \alpha)$ as defined in Ref. [28], and the strong coupling constant $\alpha_s(t)$ at two-loop level.

(2) Besides the LO hard kernel $H^{(0)}(\alpha_s)$, all the Feynman diagrams, which contribute to $H^{(1)}(\alpha_s^2)$ in the pQCD approach, should be considered. The typical Feynman diagrams which contribute to $H^{(1)}(\alpha_s^2)$ at the NLO level in the pQCD approach are shown in Figs.3-5, and can be classified into six types.

   (i) The Vertex Correction(VC): the NLO contributions from the Feynman diagrams as shown in Fig.3(a)-3(d), and have been evaluated ten years ago[21, 30, 31].

   (ii) The Quark-Loops(QL): the NLO contributions from the quark-loops as shown in Fig.3(e)-3(f), the relevant analytical formulas can be found in Ref. [21].

   (iii) The magnetic penguins (MG): the NLO contributions from the operator O_{8g}, as shown in Fig.3(g)-3(h). These Feynman diagrams are evaluated several years ago [32].

   (iv) The NLO form factors(FF): i.e. the NLO contributions to the $B \to P$ transition form factors $F_0^{B\to P}(0)$ with $P = (K, \eta_q)$ in this paper. The typical relevant Feynman diagrams are shown in Fig.4, and were calculated very recently in Ref. [14].

   (v) The NLO contributions from the spectator diagrams as shown in Figs.5(a)-5(d), which are obtained by adding a new gluon line between any two quark lines in Figs.1(c)-1(d), or by replacing the one-gluon lines with a three-gluon vertex in Figs.1(c)-1(d). Such contributions are still unknown now.

   (vi) The NLO contributions from the annihilation diagrams as shown by Fig.5(e)-5(h), which are obtained by adding a new gluon line between any two quark lines in Figs.1(e)-1(h). Such contributions are also unknown now.

The NLO contributions from the Feynman diagrams in Fig.3, the vertex corrections, the quark-loops and chromo-magnetic penguins, have been evaluated several years ago [21, 30, 32], and taken into account in our previous studies for the $B \to K\eta^{(\prime)}$ decay in Ref. [12].

The Feynman diagrams as shown in Fig.4 can provide the NLO contributions to the $B \to P$ transition form factors and have been calculated very recently in Ref. [14]. The authors of Ref.[14] calculated the NLO corrections to the $B \to \pi$ transition form factors in the leading twist in the k_T factorization theorem, and they found that the NLO part can provide a $20 - 30\%$ enhancement to the LO results for the corresponding form factors. Since π, K and $\eta^{(\prime)}$ are all pseudo-scalar mesons and have the similar forms of wave functions, it is straight forward to extend the calculations in Ref. [14] to the cases for $B \to K, \eta^{(\prime)}$ transition form factors. In this paper, we will consider the effects of the NLO part of the form factors. According to general expectation, the enhanced form factors may lead to a larger branching ratio for $B \to K\eta^{(\prime)}$ decays.

The still missing NLO parts in the pQCD approach are the $O(\alpha_s^2)$ contributions from non-factorizable spectator diagrams and annihilation diagrams, as illustrated by Figs.5(a)-5(h). The analytical calculations for these Feynman diagrams are still absent at present. But it is generally believed that the NLO contributions from these Feynman diagrams should be small

(i) For the non-factorizable spectator diagrams in Fig.1(c)-1(d), their contributions at leading order are strongly suppressed by the isospin symmetry and color-suppression

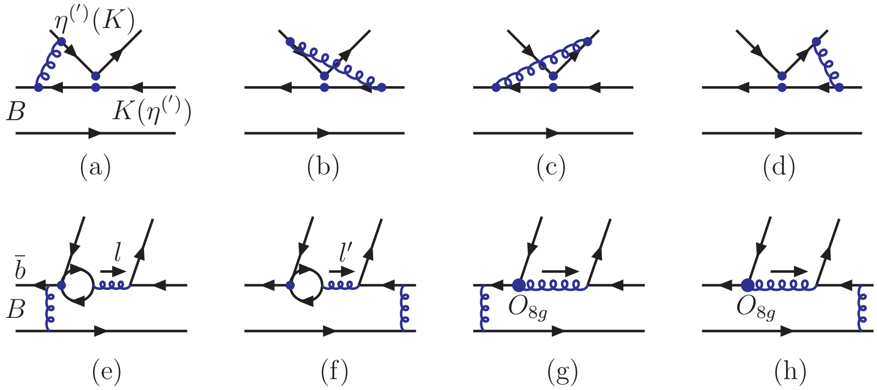

FIG. 3. The typical Feynman diagrams which provide NLO contributions to $B \to K\eta^{(\prime)}$ decays in the pQCD approach: 3(a)-3(d),the vertex corrections; 3(e)-3(f), the quark-loops; and 3(g)-3(h) the chromo-magnetic Penguins O_{8g}.

with respect to the factorizable emission diagrams Fig.1(a)-1(b). The NLO contributions from Figs.5(a)-5(d) are higher order effects on small LO quantity, and therefore should be much smaller than the LO one.

(ii) For the annihilation spectator diagrams at leading order, i.e. Figs.1(e)-1(h), they are power suppressed and generally much small with respect to the contribution from emission diagrams Fig.1(a)-1(b). The contributions from Figs.5(a)-5(d) are also the higher order corrections to the small quantity and therefore should be much smaller than its LO-part.

In next section, we will evaluate explicitly the numerical values of the individual decay amplitudes corresponding to different Feynman diagrams, and will compare the size of every parts of the total decays amplitude for the considered decays. We try to make a simple and clear comparison between the contributions from different set of Feynman diagrams or from the different sources numerically.

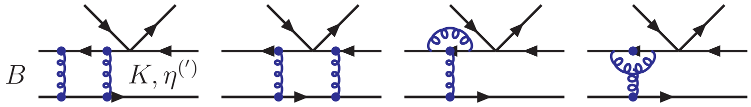

FIG. 4. The typical Feynman diagrams which may provide NLO contributions to $B \to P$ form factors.

A. The NLO contributions to $B \to K\eta^{(\prime)}$ decays

In Ref. [12], by using the ordinary FKS $\eta - \eta^{(\prime)}$ mixing scheme, we calculated the branching ratios and CP-violating asymmetries of the four $B \to K\eta^{(\prime)}$ decays at leading order and partial next-to-leading order, i.e. the NLO contributions from the feynman diagrams in Fig.3 were taken into account in Ref. [12]. For the details of the calculations about these NLO contributions and the expressions of relevant functions, one can see Ref. [12]. For the sake of reader, we here give a brief summary about those "old" NLO parts.

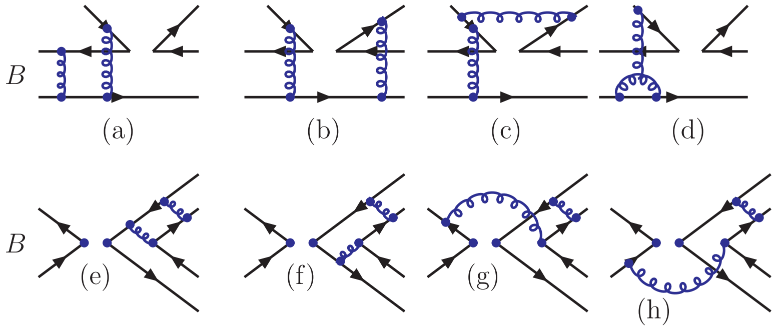

FIG. 5. The typical Feynman diagrams which may provide NLO contributions to $B \to K\eta^{(\prime)}$ decays in the pQCD approach: 5(a)-5(d), the spectator diagrams; 5(e)-5(h), the annihilation diagrams.

(a) **Vertex corrections(VC):**

The vertex corrections to the factorizable emission diagrams, as illustrated by Fig. 2(a)-2(d), have been calculated years ago in the QCD factorization appeoach[7, 30, 31]. The difference between the cases of considering or not considering the parton transverse momentum k_T are very small and can be neglected[21]. The NLO vertex corrections will be included by adding a vertex function $V_i(M)$ to the corresponding Wilson coefficients $a_i(\mu)$ [30, 31]

$$\begin{aligned} a_{1,2}(\mu) &\to a_{1,2}(\mu) + \frac{\alpha_s(\mu)}{4\pi} C_F \frac{C_{1,2}(\mu)}{3} V_{1,2}(M) \ , \\ a_i(\mu) &\to a_i(\mu) + \frac{\alpha_s(\mu)}{4\pi} C_F \frac{C_{i+1}(\mu)}{3} V_i(M), \quad for \quad i = 3, 5, 7, 9, \\ a_i(\mu) &\to a_i(\mu) + \frac{\alpha_s(\mu)}{4\pi} C_F \frac{C_{i-1}(\mu)}{3} V_i(M), \quad for \quad i = 4, 6, 8, 10, \end{aligned} \tag{48}$$

where M is the meson emitted from the weak vertex. When M is a pseudo-scalar meson, the vertex functions $V_i(M)$ can be written as [21, 31]:

$$V_i(M) = \begin{cases} 12 \ln \frac{m_b}{\mu} - 18 + \frac{2\sqrt{6}}{f_M} \int_0^1 dx \phi_M^A(x) g(x), & \text{for} \quad i = 1-4, 9, 10, \\ -12 \ln \frac{m_b}{\mu} + 6 - \frac{2\sqrt{6}}{f_M} \int_0^1 dx \phi_M^A(x) g(1-x), & \text{for} \quad i = 5, 7, \\ -6 + \frac{2\sqrt{6}}{f_M} \int_0^1 dx \phi_M^P(x) h(x), & \text{for} \quad i = 6, 8, \end{cases} \tag{49}$$

where f_M is the decay constant of the meson M, the hard-scattering functions $g(x)$ and $h(x)$ can be found in Ref. [12].

(b) **Quark loops(QL):**

The contribution from the so-called "quark-loops" is a kind of penguin correction with the four quark operators insertion, as illustrated by Fig.3(e)-3(f). We here include quark-loop amplitude from the operators $O_{1,2}$ and O_{3-6} only. The quark loops from O_{7-10} will be neglected due to their smallness.

For the $\bar{b} \to \bar{s}$ transition, the contributions from the various quark loops are given by:

$$H_{eff}^{(ql)} = - \sum_{q=u,c,t} \sum_{q'} \frac{G_F}{\sqrt{2}} V_{qb}^* V_{qs} \frac{\alpha_s(\mu)}{2\pi} C^q(\mu, l^2) \left(\bar{b}\gamma_\rho \left(1-\gamma_5\right) T^a s\right) \left(\bar{q}'\gamma^\rho T^a q'\right), \tag{50}$$

where l^2 is the invariant mass of the gluon, which attaches the quark loops in Fig. 3(e)-3(f). The functions $C^q(\mu, l^2)$ can be found in Ref. [12].

The "quark-loop" contribution to the considered $B \to K\eta^{(\prime)}$ decays can be written as[12]

$$M_{K\eta}^{(ql)} = < K\eta | \mathcal{H}_{eff}^{ql} | B > = \frac{G_F}{\sqrt{2}} \sum_{q=u,c,t} V_{qb}^* V_{qs} \left[M_{K\eta_s}^{(q)} \, F_2(\phi) + M_{\eta_q K}^{(q)} \, F_1(\phi) \right], \tag{51}$$

$$M_{K\eta'}^{(ql)} = < K\eta' | \mathcal{H}_{eff}^{(ql)} | B > = \frac{G_F}{\sqrt{2}} \sum_{q=u,c,t} V_{qb}^* V_{qs} \left[M_{K\eta_s}^{(q)} \, F_2'(\phi) + M_{\eta_q K}^{(q)} \, F_1'(\phi) \right], \tag{52}$$

where $F_{1,2}^{(\prime)}(\phi)$ are the mixing parameters and have been defined in previous sections, while the decay amplitudes $M_{K\eta_s}^{(q)}$ and $M_{\eta_q K}^{(q)}$ are of the form [12]

$$\begin{aligned} M_{K\eta_s}^{(q)} = \frac{8}{\sqrt{6}} C_F^2 m_B^4 & \int_0^1 dx_1 dx_2 \, dx_3 \int_0^\infty b_1 db_1 b_3 db_3 \, \phi_B(x_1, b_1) \\ & \cdot \left\{ \left[(1+x_3) \, \phi_K^A(x_3) \phi_{\eta_s}^A(x_2) + r_K \left(1 - 2x_3\right) \left(\phi_K^P(x_3) + \phi_K^T(x_3) \right) \phi_{\eta_s}^A(x_2) \right. \right. \\ & \left. + 2 r_{\eta_s} \phi_K^A(x_3) \phi_{\eta_s}^P(x_2) + 2 r_K r_{\eta_s} \left(\left(2 + x_3\right) \phi_K^P(x_3) - x_3 \phi_K^T(x_3) \right) \phi_{\eta_s}^P(x_2) \right] \\ & \quad \cdot E^{(q)}(t_q, l^2) h_e(x_1, x_3, b_1, b_3) \\ & + \left[2 r_K \phi_K^P(x_3) \phi_{\eta_s}^A(x_2) + 4 r_K r_{\eta_s} \phi_K^P(x_3) \phi_{\eta_s}^P(x_2) \right] \\ & \quad \left. \cdot E^{(q)}(t_q', l'^2) h_e(x_3, x_1, b_3, b_1) \right\}, \end{aligned} \tag{53}$$

for $B \to K$ transition, and

$$\begin{aligned} M_{\eta_q K}^{(q)} = \frac{8}{\sqrt{6}} C_F^2 m_B^4 & \int_0^1 dx_1 dx_2 \, dx_3 \int_0^\infty b_1 db_1 b_3 db_3 \, \phi_B(x_1, b_1) \\ & \cdot \left\{ \left[(1+x_3) \, \phi_{\eta_q}^A(x_3) \phi_K^A(x_2) + r_\eta \left(1 - 2x_3\right) \left(\phi_{\eta_q}^P(x_3) + \phi_{\eta_q}^T(x_3) \right) \phi_K^A(x_2) \right. \right. \\ & \left. + 2 r_K \phi_{\eta_q}^A(x_3) \phi_K^P(x_2) + 2 r_\eta r_K \left(\left(2 + x_3\right) \phi_{\eta_q}^P(x_3) - x_3 \phi_{\eta_q}^T(x_3) \right) \phi_K^P(x_2) \right] \\ & \quad \cdot E^{(q)}(t_q, l^2) h_e(x_1, x_3, b_1, b_3) \\ & + \left[2 r_\eta \phi_{\eta_q}^P(x_3) \phi_K^A(x_2) + 4 r_\eta r_K \phi_{\eta_q}^P(x_3) \phi_K^P(x_2) \right] \\ & \quad \left. \cdot E^{(q)}(t_q', l'^2) h_e(x_3, x_1, b_3, b_1) \right\}, \end{aligned} \tag{54}$$

for $B \to \eta$ transition. Here $r_\eta = m_0^q/m_B$ and $r_{\eta_s} = m_0^s/m_B$. The expressions of evolution functions $E^{(q)}(t_q, l^2)$ and $E^{(q)}(t_q', l'^2)$, as well as the hard functions $h_e(x_1, x_3, b_1, b_3)$ and $h_e(x_3, x_1, b_3, b_1)$ can be found in Ref. [12].

(c) **Chromo-magnetic penguins(MP):**

This is another kind of penguin correction but with the O_{8g} insertion. The corresponding effective weak Hamiltonian for $\bar{b} \to \bar{s}g$ transition is of the form[21],

$$H_{eff}^{cmp} = -\frac{G_F}{\sqrt{2}} \frac{g_s}{8\pi^2} m_b \, V_{tb}^* V_{ts} \, C_{8g}^{eff} \, \bar{b}_i \, \sigma^{\mu\nu} \, (1-\gamma_5) \, T_{ij}^a \, G_{\mu\nu}^a \, s_j, \tag{55}$$

where the effective Wilson coefficient $C_{8g}^{eff} = C_{8g} + C_5$ [21].

The total chromo-magnetic penguin contribution to the considered $B \to K\eta^{(\prime)}$ decays can be written as

$$M_{K\eta}^{(cmp)} = < K\eta | \mathcal{H}_{eff}^{cmp} | B >= -\frac{G_F}{\sqrt{2}} \, \lambda_t \, \left[M_{K\eta_s}^{(g)} \, F_2(\phi) + M_{\eta_q K}^{(g)} \, F_1(\phi) \right], \tag{56}$$

$$M_{K\eta'}^{(cmp)} = < K\eta' | \mathcal{H}_{eff}^{cmp} | B >= -\frac{G_F}{\sqrt{2}} \, \lambda_t \, \left[M_{K\eta_s}^{(g)} \, F_2'(\phi) + M_{\eta_q K}^{(g)} \, F_1'(\phi) \right], \tag{57}$$

where the mixing parameters $F_{1,2}^{(\prime)}(\phi)$ have been defined in Sec.II. The decay amplitudes $M_{K\eta_s}^{(g)}$ and $M_{\eta_q K}^{(g)}$ are obtained by evaluating the Feynman diagrams Fig. 3(g)-3(h)[12]:

$$\begin{aligned}
M_{K\eta_s}^{(g)} = & -\frac{8}{\sqrt{6}} C_F^2 m_B^6 \int_0^1 dx_1 dx_2 \, dx_3 \int_0^\infty b_1 db_1 b_2 db_2 b_3 db_3 \, \phi_B(x_1, b_1) \\
& \cdot \Big\{ \Big\{ 2(-1+x_3)\phi_{\eta_s}^A(x_2)\phi_K^A(x_3) + r_{\eta_s} x_2 (1+x_3)[-3\phi_{\eta_s}^P(x_2) + \phi_{\eta_s}^T(x_2)]\phi_K^A(x_3) \\
& + r_K[(-3+2x_3+x_3^2)\phi_K^P(x_3) + (-1+2x_3-x_3^2)\phi_K^T(x_3)]\phi_{\eta_s}^A(x_2) \\
& + 3r_{\eta_s} r_K[(-1-x_2+x_3+2x_2x_3)\phi_K^P(x_3) + (1-x_2-x_3+2x_2x_3)\phi_K^T(x_3)]\phi_{\eta_s}^P(x_2) \\
& + r_{\eta_s} r_K[(-1+x_2+x_3-2x_2x_3)\phi_K^P(x_3) + (1+x_2-x_3-2x_2x_3)\phi_K^T(x_3)]\phi_{\eta_s}^T(x_2) \Big\} \\
& \cdot E_g(t_q) h_g(A, B, C, b_1, b_3, b_2, x_3) \\
& - [4r_K \phi_{\eta_s}^A(x_2)\phi_K^P(x_3) + 2r_{\eta_s} r_K x_2 \phi_K^P(x_3)(3\phi_{\eta_s}^P(x_2) - \phi_{\eta_s}^T(x_2))] \\
& \cdot E_g(t_q') h_g(A', B', C', b_3, b_1, b_2, x_1) \Big\},
\end{aligned} \tag{58}$$

$$\begin{aligned}
M_{K\eta_q}^{(g)} = & -\frac{8}{\sqrt{6}} C_F^2 m_B^6 \int_0^1 dx_1 dx_2 \, dx_3 \int_0^\infty b_1 db_1 b_2 db_2 b_3 db_3 \, \phi_B(x_1, b_1) \\
& \cdot \Big\{ \Big\{ 2(-1+x_3)\phi_K^A(x_2)\phi_{\eta_q}^A(x_3) + r_K x_2 (1+x_3)[-3\phi_K^P(x_2) + \phi_K^T(x_2)]\phi_{\eta_q}^A(x_3) \\
& + r_\eta[(-3+2x_3+x_3^2)\phi_{\eta_q}^P(x_3) + (-1+2x_3-x_3^2)\phi_{\eta_q}^T(x_3)]\phi_K^A(x_2) \\
& + 3r_\eta r_K[(-1-x_2+x_3+2x_2x_3)\phi_{\eta_q}^P(x_3) + (1-x_2-x_3+2x_2x_3)\phi_{\eta_q}^T(x_3)]\phi_K^P(x_2) \\
& + r_\eta r_K[(-1+x_2+x_3-2x_2x_3)\phi_{\eta_q}^P(x_3) + (1+x_2-x_3-2x_2x_3)\phi_{\eta_q}^T(x_3)]\phi_K^T(x_2) \Big\} \\
& \cdot E_g(t_q) h_g(A, B, C, b_1, b_3, b_2, x_3) \\
& - [4r_\eta \phi_K^A(x_2)\phi_{\eta_q}^P(x_3) + 2r_\eta r_K x_2 \phi_{\eta_q}^P(x_3)(3\phi_K^P(x_2) - \phi_K^T(x_2))] \\
& \cdot E_g(t_q') h_g(A', B', C', b_3, b_1, b_2, x_1) \Big\},
\end{aligned} \tag{59}$$

where $r_\eta = m_0^q/m_B$, $r_{\eta_s} = m_0^s/m_B$, $r_K = m_0^K/m_B$. The explicit expressions of the evolution functions E_g and hard functions h_g in Eqs. (58,59) can be found easily in Ref. [12].

B. The form factors at NLO level

As mentioned in introduction, Li et al. derived the $k_{\rm T}$-dependent NLO hard kernel $H^{(1)}$ for the $B \to \pi$ transition form factor [14]. We here extend their results for $B \to \pi$ form factors to the ones for $B \to K$ and $B \to (\eta_q, \eta_s)$ transitions, under the assumption of $SU(3)$ flavor symmetry. As given in Eq.(56) of Ref. [14], the NLO hard kernel $H^{(1)}$ can be written as

$$\begin{aligned}
H^{(1)} &= F(x_1, x_3, \mu, \mu_f, \eta, \zeta_1) H^{(0)} \\
&= \frac{\alpha_s(\mu_f) C_F}{4\pi}\left[\frac{21}{4}\ln\frac{\mu^2}{m_B^2} - \left(\ln\frac{m_B^2}{\zeta_1^2} + \frac{13}{2}\right)\ln\frac{\mu_f^2}{m_B^2} + \frac{7}{16}\ln^2(x_1 x_3) + \frac{1}{8}\ln^2 x_1 \right.\\
&\quad + \frac{1}{4}\ln x_1 \ln x_3 + \left(2\ln\frac{m_B^2}{\zeta_1^2} + \frac{7}{8}\ln\eta - \frac{1}{4}\right)\ln x_1 + \left(\frac{7}{8}\ln\eta - \frac{3}{2}\right)\ln x_3 \\
&\quad \left. + \left(\frac{15}{4} - \frac{7}{16}\ln\eta\right)\ln\eta - \frac{1}{2}\ln\frac{m_B^2}{\zeta_1^2}\left(3\ln\frac{m_B^2}{\zeta_1^2} + 2\right) + \frac{101}{48}\pi^2 + \frac{219}{16}\right] H^{(0)}, \quad (60)
\end{aligned}$$

where the scale $\zeta_1 = 25 m_B$, $\eta = 1 - (p_1 - p_3)^2/m_B^2$ is the energy fraction carried by the meson which picks up the spectator quark. For $B \to K\eta_q, K\eta_s$ decays, the large recoil region corresponds to the energy fraction $\eta \sim O(1)$. For $B \to K\eta_c$, $\eta(K) \sim (1 - r_{\eta_c}^2)$. μ_f is the factorization scale, which is set to be the hard scales

$$t^a = \max(\sqrt{x_3\eta}\, m_B, 1/b_1, 1/b_3), \quad \mathit{or} \quad t^b = \max(\sqrt{x_1\eta}\, m_B, 1/b_1, 1/b_3), \qquad (61)$$

corresponding to the largest energy scales in Fig. 1(a) and 1(b), respectively. The renormalization scale μ is defined as [14]

$$\mu = t_s(\mu_{\rm f}) = \left\{ {\rm Exp}\left[c_1 + \left(\ln\frac{m_B^2}{\zeta_1^2} + \frac{5}{4}\right)\ln\frac{\mu_{\rm f}^2}{m_B^2}\right] x_1^{c_2}\, x_2^{c_3}\right\}^{2/21} \mu_{\rm f}, \qquad (62)$$

with the coefficients

$$\begin{aligned}
c_1 &= -\left(\frac{15}{4} - \frac{7}{16}\ln\eta\right)\ln\eta + \frac{1}{2}\ln\frac{m_B^2}{\zeta_1^2}\left(3\ln\frac{m_B^2}{\zeta_1^2} + 2\right) - \frac{101}{48}\pi^2 - \frac{219}{16}, \\
c_2 &= -\left(2\ln\frac{m_B^2}{\zeta_1^2} + \frac{7}{8}\ln\eta - \frac{1}{4}\right), \\
c_3 &= -\frac{7}{8}\ln\eta + \frac{3}{2}.
\end{aligned}$$

At the NLO level, the hard kernel function H can then be written as

$$H = H^{(0)}(\alpha_s) + H^{(1)}(\alpha_s^2) = \left[1 + F(x_1, x_3, \mu, \mu_f, \eta, \zeta_1)\right] H^{(0)}(\alpha_s). \qquad (63)$$

C. The NLO contributions to $B \to K\eta_c$ decays

For $B \to \eta_c K$ decays, the NLO contributions include two parts: (a) the NLO vertex corrections to these decays, which has been taken into account in Ref. [23]; and (b) the NLO contributions to the $B \to K$ transition form factors, which is newly known NLO part.

Since the emitted meson is $\eta_c = c\bar{c}$, the soft and collinear infrared divergences of the four vertex correction diagrams will be canceled each other. So these vertex corrections can be calculated without considering the transverse momentum effects of the quark at the end-point region, the same way as in the collinear factorrization theorem.

The NLO vertex corrections can be included through the re-definition of the Wilson coefficients:

$$\begin{aligned} a_2 &\to a_2 + \frac{\alpha_s}{4\pi} C_F \frac{C_2}{3}(-18 + 12\ln\frac{m_b}{\mu} + f_I), \\ a_i &\to a_i + \frac{\alpha_s}{4\pi} C_F \frac{C_{i+1}}{3}(-18 + 12\ln\frac{m_b}{\mu} + f_I), \quad for \quad i = 3, 9, \\ a_j &\to a_j - \frac{\alpha_s}{4\pi} C_F \frac{C_{j+1}(\mu)}{3}(-6 + 12\ln\frac{m_b}{\mu} + f_I), \quad for \quad j = 5, 7, \end{aligned} \tag{64}$$

with the function f_I is of the form

$$f_I = \frac{2\sqrt{2N_c}}{f_{\eta_c}} \int_0^1 dx \phi^{\nu}_{\eta_c}(x) \Big[\frac{3(1-2x)}{1-x} \ln x + 3(\ln(1-z) - i\pi) + \frac{2z(1-x)}{1-zx} \Big], \tag{65}$$

where $z = m^2_{\eta_c}/m^2_B$.

The NLO contributions to the $B \to K$ transition form factors can be included for the $B \to K\eta_c$ decay in the same way for $B \to K\eta^{(\prime)}$ decays.

V. NUMERICAL RESULTS AND DISCUSSIONS

A. Input parameters

We use the following input parameters [10, 11] in the numerical calculations(all masses and decay constants in units of GeV)

$$\begin{aligned} &f_B = 0.21, \quad f_K = 0.16, \quad f_{\eta_c} = 0.4874, \quad m_\eta = 0.5475, \quad m_{\eta'} = 0.9578, \\ &m_{K^0} = 0.498, \quad m_{K^+} = 0.494\text{GeV}, \quad m_{0K} = 1.7, \quad M_B = 5.28, \\ &m_b = 4.8, \quad m_c = 1.5, \quad m_{\eta_c} = 2.98, \\ &M_W = 80.41, \quad m_G = 1.376, \quad \tau_{B^0} = 1.53\text{ps}, \quad \tau_{B^+} = 1.638\text{ps}. \end{aligned} \tag{66}$$

For the CKM quark-mixing matrix, we adopt the Wolfenstein parametrization as given in Ref. [10, 11].

$$\begin{aligned} &V_{ud} = 0.9748, \quad V_{us} = \lambda = 0.2246, \quad |V_{ub}| = 3.61 \times 10^{-3}, \\ &V_{cd} = -0.225, \quad V_{cs} = 0.9748, \quad V_{cb} = 0.04197, \\ &|V_{td}| = 8.8 \times 10^{-3}, \quad V_{ts} = -0.042, \quad V_{tb} \approx 1.0, \end{aligned} \tag{67}$$

with the CKM parameters: $\lambda = 0.2246 \pm 0.0011$, $A = 0.832 \pm 0.017$, $\bar{\rho} = 0.130 \pm 0.018$, $\bar{\eta} = 0.350 \pm 0.013$.

B. Form factors at LO and NLO level

We firstly calculate and present the pQCD predictions for the form factors at zero momentum transfer for $B \to K\eta^{(\prime)}$ decays at LO and NLO level respectively. In the calculation, we consider three different mixing schemes respectively.

In this paper the form factors $F_0^{B\to\eta}(0)$ and $F_0^{B\to\eta'}(0)$ are defined as

$$\begin{aligned} F_0^{B\to\eta}(0) &= \cos\phi F_0^{B\to\eta_q}(0)_I, \\ F_0^{B\to\eta'}(0) &= \sin(\phi) F_0^{B\to\eta_q}(0)_I, \end{aligned} \tag{68}$$

in the ordinary FKS $\eta-\eta'$ mixing scheme, and

$$\begin{aligned} F_0^{B\to\eta}(0) &= \left[\cos\phi + \sin\theta\sin\theta_i(1-\cos\phi_G)\right] F_0^{B\to\eta_q}(0)_{II}, \\ F_0^{B\to\eta'}(0) &= \left[\sin\phi - \cos\theta\sin\theta_i(1-\cos\phi_G)\right] F_0^{B\to\eta_q}(0)_{II}, \end{aligned} \tag{69}$$

in the MS-2 and MS-3 mixing schemes. One should note that the form factor $F_0^{B\to\eta_q}(0)_I$ is different from $F_0^{B\to\eta_q}(0)_{II}$ since some relevant parameters in the distribution amplitudes, such as $\rho_{\eta_q} = 2m_q/m_{qq}$, are different in different mixing schemes. The pQCD predictions for the numerical values of the form factors for three different mixing schemes are all listed in Table I, and they are obtained by using the central values of all input parameters. For the relevant mixing angles, we take $\phi = 39.3^\circ$ in MS-1 mixing scheme; while we take $\theta_i = 54.7^\circ$, $\theta = -11^\circ$, $\phi = \theta + \theta_i = 43.7^\circ$ and $\phi_G = 12^\circ$ in both MS-2 and MS-3 mixing scheme. The error comes from the uncertainty of $\omega_b = 0.40 \pm 0.04$ GeV.

TABLE I. The LO and NLO pQCD predictions for the form factors of the $B \to K\eta^{(\prime)}$ decays for three different mixing schemes.

Form factors	MS	LO	NLO
$F_0^{B\to\eta_q}(0)$	1	0.20	0.26 ± 0.04
	2,3	0.28	0.33 ± 0.06
$F_0^{B\to K}(0)$	all	0.37	$0.43^{+0.07}_{-0.05}$

From the numerical values of the form factors in Table. I, we can see that (a) the form factors are the same for the η-η'-G mixing scheme and the η-η'-G-η_c mixing scheme, since the η_c component in the η-η'-G-η_c mixing scheme does not affect the evaluation of the form factors $F_0^{B\to\eta^{(\prime)}}(0)$ and $F_0^{B\to K}(0)$; and (b) the NLO contributions also provide $\sim 20\%$ enhancements to the corresponding form factors.

C. $Br(B \to K\eta^{(\prime)})$ in η-η' mixing scheme

In the B-rest frame, the branching ratio of a general $B \to M_2M_3$ decay can be written as

$$Br(B \to M_2M_3) = \tau_B \, \frac{1}{16\pi m_B} \, \chi \, \left|\mathcal{M}(B \to M_2M_3)\right|^2, \tag{70}$$

where τ_B is the lifetime of the B meson, $\chi \approx 1$ is the phase space factor and equals to unit when the masses of final state light mesons are neglected.

Using the input parameters and the wave functions as given in previous sections, it is straightforward to calculate the CP-averaged branching ratios for the considered four $B \to K\eta^{(\prime)}$ decays in different mixing schemes. For the case of the ordinary $\eta - \eta'$ mixing scheme, the pQCD predictions are listed in Table. II, where the label "NLO-1" refers to the pQCD predictions with the inclusion of the same set of NLO contributions as in Ref. [12]. The label NLO in Table III means all currently known NLO contributions are included, especially the NLO part of the form factor obtained by evaluating the Feynman diagrams as shown in Fig.4 [14]. For comparison, we also list the corresponding experimental measurements [10] and the theoretical predictions in the pQCD approach [12] and in the QCDF approach [31].

TABLE II. The pQCD predictions for the branching ratios (in unit of 10^{-6}) in the ordinary η-η' mixing scheme with $\phi = 39.3°$. The label NLO means all currently known NLO contributions are included.

Channel	LO	NLO-1	NLO	Data[10]	pQCD[12]	QCDF[31]
$B^0 \to K^0\eta$	2.12	2.76	$2.62^{+3.6}_{-1.7}$	$1.23^{+0.27}_{-0.24}$	$2.1^{+2.6}_{-1.5}$	$1.1^{+2.4}_{-1.5}$
$B^0 \to K^0\eta'$	27.9	48.3	$57.2^{+23.7}_{-17.0}$	66.1 ± 3.1	$50.3^{+16.8}_{-10.6}$	$46.5^{+41.9}_{-22.0}$
$B^+ \to K^+\eta$	3.83	3.78	$4.0^{+3.8}_{-2.2}$	$2.4^{+0.22}_{-0.21}$	$3.2^{+3.2}_{-1.8}$	$1.9^{+3.0}_{-1.9}$
$B^+ \to K^+\eta'$	30.3	49.8	$58.7^{+24.0}_{-17.2}$	71.1 ± 2.6	$51.0^{+18.0}_{-10.9}$	$49.1^{+45.2}_{-23.6}$

Of course, the NLO pQCD predictions for the CP-averaged branching ratios still have large theoretical uncertainties. If we take into account the effects of the uncertainties of the main input parameters, we find that

$$\begin{aligned}
Br(\ B^0 \to K^0\eta) &= \left[2.62^{+1.22}_{-0.78}(\omega_b)^{+2.49}_{-1.04}(m_s)^{+0.52}_{-0.48}(f_B)^{+1.37}_{-1.04}(a_2^\eta)\right] \times 10^{-6}, \\
Br(\ B^0 \to K^0\eta') &= \left[57.2^{+16.1}_{-11.2}(\omega_b)^{+12.6}_{-7.00}(m_s)^{+11.4}_{-10.4}(f_B)^{+3.49}_{-2.42}(a_2^\eta)\right] \times 10^{-6}, \\
Br(\ B^+ \to K^+\eta) &= \left[3.97^{+1.67}_{-1.13}(\omega_b)^{+2.97}_{-1.30}(m_s)^{+0.79}_{-0.72}(f_B)^{+1.57}_{-1.20}(a_2^\eta)\right] \times 10^{-6}, \\
Br(\ B^+ \to K^+\eta') &= \left[58.7^{+16.2}_{-11.2}(\omega_b)^{+13.0}_{-7.20}(m_s)^{+11.7}_{-10.6}(f_B)^{+3.17}_{-2.18}(a_2^\eta)\right] \times 10^{-6}, \qquad (71)
\end{aligned}$$

where the major errors are induced by the uncertainties of $\omega_b = 0.4 \pm 0.04$ GeV, $m_s = 0.13 \pm 0.03$ GeV, $f_B = 0.21 \pm 0.02$GeV and Gegenbauer moment $a_2^\eta = 0.44 \pm 0.22$ (here a_2^η denotes $a_2^{\eta_q}$ or $a_2^{\eta_s}$), respectively. The total theoretical errors in the NLO pQCD predictions as shown in the fourth column of Table II are obtained by adding the four individual theoretical errors in quadrature. from the numerical results as given in Eq. (71) and Table II we fnd the following points

(i) By comparing the predictions as listed in "NLO-1" column and "NLO" column, one can see that the inclusion of the NLO contributions to the form factors can provide about 18% enhancement to $Br(B \to K\eta')$, the gap between the pQCD predictions and the measured values therefore become narrow effectively, but there is still a small difference between the central values of the pQCD predictions and the data.

(ii) For $B \to K\eta$ decays, however, the pQCD predictions for their branching ratios remain basically unchanged after the inclusion of NLO part of the form factors. Although the NLO pQCD predictions for $Br(B \to K\eta)$ are consistent with the data within one standard deviation, but the central values of the NLO pQCD predictions are still larger than the measured values by almost a factor of 2.

(iii) The pQCD predictions as given in the NLO-1 column agree well with those presented in Ref. [12](i.e. the results as listed in the "pQCD" column of Table II), the small differences are induced by the variations of some input parameters, such as the CKM matrix elements.

(iv) Although the NLO pQCD predictions for $Br(B \to K\eta)$ and $Br(B \to K\eta')$ are consistent with the data within one standard deviation, but we here can not provide a good interpretation for the observed pattern of $Br(B \to k\eta^{(\prime)})$ in the FKS η-η' mixing scheme.

D. $Br(B \to K\eta^{(\prime)})$ in η-η'-G mixing scheme

In the η-η'-G mixing scheme, by using the input parameters and the wave functions as given in previous sections and fixing the mixing parameters $\theta = -11^\circ, \phi = 43.7^\circ$ and $\phi_G = 12^\circ$, we find the LO and NLO pQCD predictions for the CP-averaged branching ratios as listed in Table III. As a comparison, we also show the measured values and the QCDF predictions as given in Ref. [31] in last two columns of the Table III.

TABLE III. The same as in Table I but for the case of the η-η'-G mixing scheme with the mixing parameters $\phi = 43.7^\circ, \theta = -11^\circ, \theta_i = 54.7^\circ$ and $\phi_G = 12^\circ$.

Channel	LO	NLO-1	NLO	Data[10]	QCDF[31]
$B^0 \to K^0\eta$	0.90	1.15	$1.13^{+2.0}_{-1.0}$	$1.23^{+0.27}_{-0.24}$	$1.1^{+2.4}_{-1.5}$
$B^0 \to K^0\eta'$	35.2	57.4	$66.5^{+25.9}_{-15.4}$	66.1 ± 3.1	$46.5^{+41.9}_{-22.0}$
$B^+ \to K^+\eta$	1.98	2.10	$2.36^{+2.6}_{-1.5}$	$2.36^{+0.22}_{-0.21}$	$1.9^{+3.0}_{-1.9}$
$B^+ \to K^+\eta'$	38.9	58.3	$67.3^{+26.0}_{-19.4}$	71.1 ± 2.6	$49.1^{+45.2}_{-23.6}$

The NLO pQCD predictions with the inclusion of the major theoretical errors are the following

$$\begin{aligned}
Br(\ B^0 \to K^0\eta) &= \left[1.13^{+0.50}_{-0.32}(\omega_b)^{+1.60}_{-0.67}(m_s)^{+0.23}_{-0.20}(f_B)^{+0.99}_{-0.69}(a_2^\eta)\right] \times 10^{-6}, \\
Br(\ B^0 \to K^0\eta') &= \left[66.5^{+19.6}_{-13.6}(\omega_b)^{+9.9}_{-6.4}(m_s)^{+13.3}_{-12.1}(f_B)^{+3.0}_{-2.1}(a_2^\eta)\right] \times 10^{-6}, \\
Br(\ B^+ \to K^+\eta) &= \left[2.36^{+0.97}_{-0.61}(\omega_b)^{+2.05}_{-0.94}(m_s)^{+0.47}_{-0.43}(f_B)^{+1.25}_{-0.90}(a_2^\eta)\right] \times 10^{-6}, \\
Br(\ B^+ \to K^+\eta') &= \left[67.3^{+19.6}_{-13.5}(\omega_b)^{+10.2}_{-6.4}(m_s)^{+13.4}_{-12.2}(f_B)^{+2.7}_{-1.8}(a_2^\eta)\right] \times 10^{-6}.
\end{aligned} \tag{72}$$

Analogous to the case of MS-1, the major theoretical errors in MS-2 mixing scheme are still induced by the uncertainties of the input parameters: $\omega_b = 0.4 \pm 0.04$ GeV, $m_s = 0.11 \pm 0.02$ GeV, $f_B = 0.21 \pm 0.02$GeV and Gegenbauer moment $a_2^\eta = 0.44 \pm 0.22$. The total theoretical errors of the NLO pQCD predictions in the fourth column of Table

III are obtained by adding the four individual theoretical errors in quadrature. One can see from the numerical results in Eq. (72) and Table III that

(i) In the η-η'-G mixing scheme, the glueball part play an important rule in improving the agreement between the pQCD predictions with the data. Even at the leading order, the pQCD predictions for $Br(B \to K\eta')$ ($Br(B \to K\eta)$) become larger (smaller) than those in the case of MS-1, the corresponding changes are what we want to interpret the data.

(ii) For $B^0 \to K^0\eta'$ ($B^+ \to K^+\eta'$) decay, the NLO contribution provide a 89% (73%) enhancement to its branching ratio with respect to the LO prediction. The NLO part of the form factors along provide a 23% enhancement to the corresponding branching ratios. The NLO pQCD predictions for both $Br(B^0 \to K^0\eta')$ and $Br(B^+ \to K^+\eta')$ are now in full agreement with the data.

(iii) For both $B^0 \to K^0\eta$ and $B^+ \to K^+\eta$ decays, the NLO enhancements are small in size, the agreement between the pQCD predictions and the data also improved effectively due to the inclusion of the all known NLO contributions.

(iv) For all four $B \to K\eta^{(\prime)}$ decays in consideration, the differences between the numerical values as listed in the NLO-1 column and NLO column in Table III show the effects of the inclusion of the NLO part of the form factors. It is easy to see that the NLO pQCD predictions for the branching ratios become in perfect agreement with the measured values due to the contribution from the guleball component in the η-η'-G mixing scheme and the inclusion of the NLO contributions.

E. $Br(B \to K\eta^{(\prime)})$ in “η-η'-G-η_c” mixing scheme

In the “η-η'-G-η_c” mixing scheme, by using the input parameters and the wave functions as given in previous sections and fixing the mixing parameters $\theta = -11^\circ, \phi = 43.7^\circ$, $\phi_G = 12^\circ$ and $\phi_Q = 11^\circ$, we find the LO and NLO pQCD predictions for the CP-averaged branching ratios as listed in Table IV.

TABLE IV. The same as in Table I but for the case of the “η-η'-G-η_c” mixing scheme. The label NLO means all known NLO contributions are included.

Channel	LO	NLO-1	NLO	Data[10]	QCDF[31]
$B^0 \to K^0\eta$	0.67	0.87	$0.82^{+1.8}_{-0.8}$	$1.23^{+0.27}_{-0.24}$	$1.1^{+2.4}_{-1.5}$
$B^0 \to K^0\eta'$	43.5	55.6	$64.8^{+26.8}_{-20.4}$	66.1 ± 3.1	$46.5^{+41.9}_{-22.0}$
$B^+ \to K^+\eta$	1.50	2.00	$2.19^{+2.5}_{-1.4}$	$2.36^{+0.22}_{-0.21}$	$1.9^{+3.0}_{-1.9}$
$B^+ \to K^+\eta'$	51.7	56.2	$65.2^{+27.0}_{-20.0}$	71.1 ± 2.6	$49.1^{+45.2}_{-23.6}$

In the “η-η'-G-η_c” mixing scheme, the contributions from the decay chain $B \to K\eta_c \to K\eta^{(\prime)}$ will be included. The NLO pQCD predictions for the CP-averaged branching ratios with the major theoretical errors are of the form

$$\begin{aligned} Br(\ B^0 \to K^0\eta) &= \left[0.82^{+0.29}_{-0.18}(\omega_b)^{+1.47}_{-0.57}(m_s)^{+0.17}_{-0.14}(f_B)^{+0.92}_{-0.55}(a_2^\eta)\right] \times 10^{-6}, \\ Br(\ B^0 \to K^0\eta') &= \left[64.8^{+21.2}_{-14.7}(\omega_b)^{+10.3}_{-6.5}(m_s)^{+12.9}_{-11.8}(f_B)\right] \times 10^{-6}, \\ Br(\ B^+ \to K^+\eta) &= \left[2.19^{+0.75}_{-0.54}(\omega_b)^{+2.06}_{-0.95}(m_s)^{+0.44}_{-0.40}(f_B)^{+1.19}_{-0.86}(a_2^\eta)\right] \times 10^{-6}, \\ Br(\ B^+ \to K^+\eta') &= \left[65.2^{+21.2}_{-14.7}(\omega_b)^{+10.6}_{-6.8}(m_s)^{+13.0}_{-11.8}(f_B)\right] \times 10^{-6}. \end{aligned} \tag{73}$$

Analogous to the cases of η-η' and η-η'-G mixing schemes, the major errors here are also induced by the uncertainties of ω_b, m_s, f_B and Gegenbauer coefficient a_2^η, respectively. For $B \to K\eta'$ decays, however, the error induced by the uncertainty of $a_2^\eta = 0.44 \pm 0.22$ are very small and have been neglected. The total theoretical errors of the NLO pQCD predictions in the fourth column of Table IV are obtained by adding the individual theoretical errors in quadrature.

From Table IV, one can see that the NLO pQCD predictions for $Br(B \to K\eta')$ also agree well with the data. For $B \to K\eta$ decays, although the central values of the NLO pQCD predictions for $Br(B \to K\eta)$ are a little smaller than the measured values, but they are still consistent with the data within one standard deviation. Since the values of the relevant mixing parameters $F_C(\theta, \phi_G, \phi_Q)$ and $F_C'(\theta, \phi_G, \phi_Q)$ as defined in Eq. (47) are all very small,

$$F_C(\theta, \phi_G, \phi_Q) = 0.0076, \quad F_C'(\theta, \phi_G, \phi_Q) = 0.039, \tag{74}$$

for $(\theta, \phi_G, \phi_Q) = (-11^\circ, 12^\circ, 11^\circ)$, the η_c contributions to the $B \to K\eta^{(\prime)}$ decays are indeed very small.

F. CP-violating asymmetries

Now we turn to the evaluations of the CP-violating asymmetries of $B \to K\eta^{(\prime)}$ decays in pQCD approach. For $B^+ \to K^+\eta^{(\prime)}$ decays, the direct CP-violating asymmetries $\mathcal{A}_{CP}$ can be defined as:

$$\mathcal{A}_{CP}^{dir} = \frac{\Gamma(\bar{B}^0 \to \bar{f}) - \Gamma(B^0 \to f)}{\Gamma(\bar{B}^0 \to \bar{f}) + \Gamma(B^0 \to f)} = \frac{|\overline{\mathcal{M}}_{\bar{f}}|^2 - |\mathcal{M}_f|^2}{|\overline{\mathcal{M}}_{\bar{f}}|^2 + |\mathcal{M}_f|^2}, \tag{75}$$

Using the input parameters and the wave functions as given in previous sections, it is easy to calculate the direct CP-violating asymmetries for the considered decays, which are listed in Table V. The major theoretical errors as given in Table V are induced by the uncertainties of input parameters of ω_b, m_s and a_2^η. As a comparison, we also list currently available data [10] and the corresponding QCDF predictions [31]. The label NLO means that all known NLO contributions are taken into account. For $B^\pm \to K^\pm\eta$ decays, there is a large direct CP asymmetry ($\mathcal{A}_{CP}^{dir}$), due to the destructive interference between the penguin amplitude and the tree amplitude.

From the pQCD predictions and the relevant data as listed in Table V, one can see that

(i) For $B^\pm \to K^\pm\eta$ decays, the LO pQCD predictions for $\mathcal{A}_{CP}^{dir}$ in all three mixing schemes have an opposite sign with the measured value. The inclusion of the NLO

TABLE V. The LO and NLO pQCD predictions for the direct CP asymmetries $\mathcal{A}_{CP}^{dir}(B^\pm \to K^\pm \eta)$ and $\mathcal{A}_{CP}^{dir}(B^\pm \to K^\pm \eta')$ in the three different mixing schemes (in units of 10^{-2}).

Mode	MS	LO	NLO	Data[10]	QCDF[31]
$\mathcal{A}_{CP}^{dir}(K^\pm \eta)$	1	10.0	$-25.2^{+2.7}_{-1.8}(\omega_b)^{+10.9}_{-12.3}(m_s)^{+8.0}_{-12.2}(a_2^\eta)$	-37 ± 8	$-18.9^{+29.0}_{-30.0}$
	2	31.1	$-22.9^{+7.6}_{-5.2}(\omega_b)^{+11.6}_{-16.7}(m_s)^{+6.3}_{-7.6}(a_2^\eta)$		
	3	42.4	$-2.8^{+8.5}_{-8.5}(\omega_b)^{+1.9}_{-3.3}(m_s)^{+8.4}_{-3.3}(a_2^\eta)$		
$\mathcal{A}_{CP}^{dir}(K^\pm \eta')$	1	-10.4	$-4.4^{+0.7}_{-0.6}(\omega_b)^{+1.1}_{-0.8}(m_s)^{+1.5}_{-1.3}(a_2^\eta)$	$1.3^{+1.6}_{-1.7}$	$-9.0^{+10.6}_{-16.2}$
	2	-12.2	$-5.5^{+0.8}_{-0.8}(\omega_b)^{+0.9}_{-0.7}(m_s)^{+1.5}_{-1.5}(a_2^\eta)$		
	3	-9.0	$-2.3^{+1.1}_{-1.1}(\omega_b)^{+0.4}_{-0.4}(m_s)^{+1.4}_{-1.6}(a_2^\eta)$		

contributions changed the sign of the pQCD prediction for $\mathcal{A}_{CP}^{dir}$, the NLO pQCD predictions for $\mathcal{A}_{CP}^{dir}(B^\pm \to K^\pm \eta)$ in the cases of MS-1 and MS-2 are now becoming consistent with the data within one standard deviation. In the "η-η'-G" mixing scheme, for example, the NLO pQCD predictions are of the form

$$\begin{aligned} \mathcal{A}_{CP}^{dir}(B^\pm \to K^\pm \eta) &= -22.9^{+15.2}_{-19.1} \times 10^{-2}, \\ \mathcal{A}_{CP}^{mix}(B^\pm \to K^\pm \eta') &= -5.5^{+1.9}_{-1.8} \times 10^{-2}, \end{aligned} \tag{76}$$

where the individual errors as shown in Table V are added in quadrature.

(ii) In the case of MS-3, however, the pQCD prediction for $\mathcal{A}_{CP}^{dir}(B^\pm \to K^\pm \eta)$ changed its sign after the inclusion of the NLO contributions. The NLO pQCD prediction is of the form

$$\mathcal{A}_{CP}^{dir}(B^\pm \to K^\pm \eta') = -2.8^{+10.7}_{-9.7} \times 10^{-2}, \tag{77}$$

which is still much smaller than the measured value in magnitude. There is a clear difference between the pQCD prediction and the data for $\mathcal{A}_{CP}^{dir}(B^\pm \to K^\pm \eta')$ in the "η-η'-G-η_c" mixing scheme.

(iii) For $B^\pm \to K^\pm \eta'$ decays, the measured value of $\mathcal{A}_{CP}^{dir}(K^\pm \eta') = 1.3^{+1.6}_{-1.7} \times 10^{-2}$ is consistent with zero. The NLO pQCD predictions in three different mixing schemes agree well with the data within one standard deviation, while the consistency between the pQCD predictions and the data are improved effectively by the inclusion of the NLO contributions.

As to the CP-violating asymmetries for the neutral decays $B^0 \to K^0 \eta^{(\prime)}$, the effects of $B^0 - \bar{B}^0$ mixing should be considered. The CP-violating asymmetry of $B^0(\bar{B}^0) \to K^0 \eta^{(\prime)}$ decays are time dependent and can be defined as

$$A_{CP} \equiv \frac{\Gamma_{\overline{B}_d^0 \to f}(\Delta t) - \Gamma_{B_d^0 \to f}(\Delta t)}{\Gamma_{\overline{B}_d^0 \to f}(\Delta t) + \Gamma_{B_d^0 \to f}(\Delta t)} = \mathcal{C}_f \cos(\Delta m \Delta t) + \mathcal{S}_f \sin(\Delta m \Delta t), \tag{78}$$

where Δm is the mass difference between the two B_d^0 mass eigenstates, $\Delta t = t_{CP} - t_{tag}$ is the time difference between the tagged B^0 ($\overline{B}^0$) and the accompanying $\overline{B}^0$ (B^0) with opposite b flavor decaying to the final CP-eigenstate f_{CP} at the time t_{CP}. The direct and mixing induced CP-violating asymmetries $\mathcal{C}_f$ (or $\mathcal{A}_f$ in term of Belle Collaboration) and $\mathcal{S}_f$ can be written as

$$\mathcal{A}_{CP}^{dir} = \mathcal{C}_f \equiv \frac{|\lambda|^2 - 1}{1 + |\lambda|^2}, \qquad \mathcal{A}_{CP}^{mix} = \mathcal{S}_f \equiv \frac{2Im(\lambda)}{1 + |\lambda|^2}, \tag{79}$$

with the CP-violating parameter λ

$$\lambda \equiv \left(\frac{q}{p}\right)_d \cdot \frac{\langle f|H_{eff}|\overline{B}^0\rangle}{\langle f|H_{eff}|B^0\rangle}. \tag{80}$$

By integrating the time variable t, one finds the total CP asymmetries for $B^0 \to K^0\eta^{(\prime)}$ decays,

$$\mathcal{A}_{CP}^{tot} = \frac{1}{1+x^2}\mathcal{A}_{CP}^{dir} + \frac{x}{1+x^2}\mathcal{A}_{CP}^{mix}, \tag{81}$$

where $x = \Delta m/\Gamma = 0.774$ [11].

In Table VI, we show the LO and NLO pQCD predictions for the direct, the mixing-induced, and the total CP asymmetries for $B^0 \to K_S^0\eta^{(\prime)}$ decays in three different mixing schemes. Analogous to the NLO pQCD predictions for the branching ratios, the label "NLO" here means the inclusion of all currently known NLO contributions are taken into account.

From the pQCD predictions and currently available experimental measurements for the CP-violating asymmetries of $B^0 \to K_S^0\eta^{(\prime)}$ decays, one can see that:

(i) Unlike the cases for the branching ratios, the pQCD predictions for the CP-violating asymmetries of the neutral $B^0 \to K_S^0\eta^{(\prime)}$ decays are not sensitive to both the NLO contributions and the choice of the mixing schemes.

(ii) The NLO pQCD predictions for $\mathcal{A}_{CP}^{dir}(B^0 \to K_S^0\eta')$ and $\mathcal{A}_{CP}^{mix}(B^0 \to K_S^0\eta')$ have small theoretical error and agree very well with the measured values:

$$\begin{aligned}\mathcal{A}_{CP}^{dir}(B^0 \to K_S^0\eta') &= (3.3 \pm 0.3(\text{theory})) \times 10^{-2},\\ \mathcal{A}_{CP}^{mix}(B^0 \to K_S^0\eta') &= (70.3 \pm 0.5(\text{theory})) \times 10^{-2},\end{aligned} \tag{82}$$

while the measured values are $(1-9)\%$ and $(64 \pm 11)\%$, respectively.

(iii) The pQCD predictions of $\mathcal{A}_{CP}^{dir}(B^0 \to K_S^0\eta) \sim -16\%$ and $\mathcal{A}_{CP}^{mix}(B^0 \to K_S^0\eta) \sim 67\%$ will be tested by the LHCb and the forthcoming Super-B experiments.

TABLE VI. The pQCD predictions for the direct-, mixing-induced and total CP asymmetries (in units of 10^{-2}) for $B^0 \to K^0\eta^{(\prime)}$ decays in three different mixing schemes, and the world averages as given by HFAG [10].

Mode	MS	LO	NLO	Data
$\mathcal{A}_{CP}^{dir}(B^0 \to K_S^0\eta)$	1	-4.6	$-11.1^{+0.7}_{-0.7}(\omega_b)^{+2.9}_{-2.0}(m_s)^{+2.6}_{-3.3}(a_2^\eta)$	–
	2	-6.6	$-16.0^{+0.9}_{-0.8}(\omega_b)^{+5.8}_{-7.8}(m_s)^{+5.3}_{-11.9}(a_2^\eta)$	–
	3	-7.8	$-19.4^{+0.8}_{-0.0}(\omega_b)^{+8.1}_{-16.2}(m_s)^{+7.4}_{-16.7}(a_2^\eta)$	–
$\mathcal{A}_{CP}^{mix}(B^0 \to K_S^0\eta)$	1	69.3	$66.3^{+0.5}_{-0.3}(\omega_b)^{+2.4}_{-3.3}(m_s)^{+2.2}_{-3.9}(a_2^\eta)$	–
	2	69.9	$66.7^{+1.5}_{-1.5}(\omega_b)^{+2.6}_{-6.5}(m_s)^{+2.2}_{-5.2}(a_2^\eta)$	–
	3	70.3	$69.5^{+2.1}_{-2.0}(\omega_b)^{+0.8}_{-2.8}(m_s)^{+2.6}_{-0.5}(a_2^\eta)$	–
$\mathcal{A}_{CP}^{tot}(B^0 \to K_S^0\eta)$	1	30.6	$25.2^{+0.3}_{-0.2}(\omega_b)^{+3.0}_{-2.9}(m_s)^{+2.7}_{-4.0}(a_2^\eta)$	–
	2	29.7	$22.3^{+0.2}_{-0.0}(\omega_b)^{+4.8}_{-8.1}(m_s)^{+4.4}_{-9.9}(a_2^\eta)$	–
	3	29.2	$21.6^{+1.5}_{-1.0}(\omega_b)^{+5.5}_{-11.5}(m_s)^{+4.9}_{-9.2}(a_2^\eta)$	–
$\mathcal{A}_{CP}^{dir}(B^0 \to K_S^0\eta')$	1	1.1	$3.4^{+0.2}_{-0.2}(\omega_b)^{+0.1}_{-0.2}(m_s)^{+0.1}_{-0.1}(a_2^\eta)$	–
	2	1.0	$3.3^{+0.1}_{-0.2}(\omega_b)^{+0.1}_{-0.1}(m_s)^{+0.1}_{-0.1}(a_2^\eta)$	1 ± 9
	3	0.9	$3.5^{+0.1}_{-0.1}(\omega_b)^{+0.1}_{-0.2}(m_s)^{+0.2}_{-0.2}(a_2^\eta)$	–
$\mathcal{A}_{CP}^{mix}(B^0 \to K_S^0\eta')$	1	70.7	$69.8^{+0.1}_{-0.1}(\omega_b)^{+0.2}_{-0.1}(m_s)^{+0.2}_{-0.2}(a_2^\eta)$	–
	2	70.8	$70.0^{+0.1}_{-0.1}(\omega_b)^{+0.1}_{-0.1}(m_s)^{+0.1}_{-0.1}(a_2^\eta)$	64 ± 11
	3	70.8	$70.5^{+0.1}_{-0.1}(\omega_b)^{+0.1}_{-0.0}(m_s)^{+0.1}_{-0.1}(a_2^\eta)$	–
$\mathcal{A}_{CP}^{tot}(B^0 \to K_S^0\eta')$	1	34.9	$35.9^{+0.2}_{-0.2}(\omega_b)^{+0.0}_{-0.0}(m_s)^{+0.0}_{-0.0}(a_2^\eta)$	–
	2	34.9	$36.0^{+0.1}_{-0.2}(\omega_b)^{+0.0}_{-0.0}(m_s)^{+0.0}_{-0.0}(a_2^\eta)$	–
	3	34.8	$36.3^{+0.1}_{-0.1}(\omega_b)^{+0.1}_{-0.1}(m_s)^{+0.1}_{-0.1}(a_2^\eta)$	–

G. Relative strength of the contributions from different sources

In the pQCD approach at leading order, we generally expect that (a) the factorizable emission diagrams Figs.1(a) and 1(b) provide the dominant contribution to the considered $B \to K\eta^{(\prime)}$; (b) the non-factorizable spectator diagrams Figs.1(c) and 1(d) are strongly suppressed by both the isospin cancelation and the color-suppression and therefore play a minor role; and (c) the annihilation diagrams Fig.1(e)-1(h) are generally power suppressed in magnitude, but may provide a large strong phase to produce large CP-violating asymmetries for some decay modes.

In the pQCD approach at next-to-leading order, as presented in previous sections, we assume that those currently known NLO contributions are the dominant part of the NLO contribution, while the still missing part from the spectator and annihilation diagrams Figs.5(a)-5(h) is small in size and can be neglected safely. Of course, this assumption should be examined properly before the calculations for those missed part become available. For this purpose, we try to check about the relative strength of the LO or NLO contributions coming from different sources.

If the LO contributions ($\propto \mathcal{O}(\alpha_s)$) from Figs.1(c)-1(d) and Figs.1(e)-1(h) are already much smaller in size when compared with those from the emission diagrams Figs.1(a)-

1(b), it is reasonable for us to assume that the still missing next-to-leading order $O(\alpha_s^2)$ corrections coming from Figs.5(a)-5(h) should be smaller than their counterparts at leading order, and therefore much smaller than those dominant LO contribution and therefore can be neglected safely.

In order to check these general expectations or assumptions correct or not, we here will firstly decompose the LO decay amplitude $\mathcal{M}_{LO}$ into different parts according to the corresponding Feynman diagrams, and then make numerical evaluations for each part and compare their magnitude directly. We try to make a simple and clear numerical comparison for the contributions from different sources

For $B^+ \to K^+\eta$ decay in the η-η' mixing scheme, for example, its decay amplitude $\mathcal{M}(B^+ \to K^+\eta)$ at leading order as given in Eq. (43) [1] can be written as a sum of three parts

$$\mathcal{M}_{LO}(B^+ \to K^+\eta) = \mathcal{M}^{a+b}(K^+\eta) + \mathcal{M}^{c+d}(K^+\eta) + \mathcal{M}^{anni}(K^+\eta), \tag{83}$$

where the decay amplitude $\mathcal{M}^{a+b}$ are obtained by evaluating the dominant emission diagrams Figs.1(a)-1(b), $\mathcal{M}^{c+d}$ refers to the LO contribution from the spectator diagrams Figs.1(c)-1(d), while $\mathcal{M}^{anni}$ denotes the LO contribution from the annihilation diagrams Figs.1(e)-1(h).

By using the central values of the input parameters and the relevant wave functions, we make the numerical calculations and find the results (in unit of 10^{-4})

$$\begin{aligned}\mathcal{M}_{LO}(B^+ \to K^+\eta) &= \underbrace{-1.76 - i0.37}_{\mathcal{M}^{a+b}} + \underbrace{0.065 - i0.14}_{\mathcal{M}^{c+d}} + \underbrace{0.01 + i0.57}_{\mathcal{M}^{anni}} \\ &= -1.67 - i0.062, \end{aligned} \tag{84}$$

it is easy to see that (a) $\mathcal{M}^{a+b}$ is indeed large and dominant; (b) $\mathcal{M}^{c+d}$ is negligibly smaller than both $\mathcal{M}^{a+b}$ and $\mathcal{M}^{anni}$; and (c) the real part of $\mathcal{M}^{anni}$ is close to zero, but its imaginary is large and interferes destructively with $\mathcal{M}^{a+b}$.

Since the branching ratio of the considered decays are proportional to the square of the decays amplitude $|\mathcal{M}|^2$, as shown by Eq. (70), we can define the relative strength of the individual contribution from different sources as the ratio R_{LO}:

$$R_{LO}(K^+\eta) = |\mathcal{M}^{a+b}|^2 : |\mathcal{M}^{c+d}|^2 : |\mathcal{M}^{anni}|^2 : |\mathcal{M}_{LO}|^2 = 3.23 : 0.02 : 0.33 : 2.79. \tag{85}$$

One can see directly from above numbers that the contributions from $\mathcal{M}^{c+d}$ is less than 1% and can be neglected safely, while the contributions from $\mathcal{M}^{anni}$ is also small in magnitude, around 10% of the dominant contribution from emission diagram Figs.1(a)-1(b).

Using the same methods, we make the similar decompositions and numerical calculations for the remaining three decay modes $B^0 \to K^0\eta^{(\prime)}$ and $B^+ \to K^+\eta'$, and find the numerical values of the decay amplitudes and the relative strength. We make the calculations in both the η-η' and η-η'-G mixing scheme and show all the numerical results in Table VII. For the case of each mixing scheme we use the same input parameters as those used in the calculation for branching ratios in Sec.V-C and V-D , respectively.

From the numerical results as shown in Table VII, we find the following points:

---

[1] In the η-η' and η-η'-G mixing scheme, the last term $\mathcal{M}(B \to \eta_c K) \cdot F_c(\theta, \phi_G, \phi_Q)$ in Eq. (43) is absent.

TABLE VII. The LO pQCD predictions for the numerical values (in unit of 10^{-4}) of the individual and total decay amplitudes of $B^0 \to K^0 + \eta^{(\prime)}$ and $B^+ \to K^+\eta^{(\prime)}$ decays, and in the η-η' and η-η'-G mixing scheme.

Decay	MS	$\mathcal{M}^{a+b}$	$\mathcal{M}^{c+d}$	$\mathcal{M}^{anni}$	$\mathcal{M}_{LO}$	R_{LO}
$K^0\eta$	1	$-1.30 - i0.04$	$0.06 - i0.11$	$-0.06 + i0.53$	$-1.30 + i0.47$	1.69 : 0.01 : 0.29 : 1.91
	2	$-0.80 + i0.03$	$0.03 - i0.07$	$0.01 + i0.54$	$-0.76 + i0.51$	0.63 : 0.01 : 0.30 : 0.83
$K^0\eta'$	1	$3.42 - i0.03$	$0.25 - i0.47$	$-0.07 - i2.85$	$3.40 - i3.29$	11.7 : 0.29 : 8.1 : 22.4
	2	$4.12 + i0.03$	$0.24 - i0.45$	$-0.03 - i2.94$	$4.32 - i3.37$	17.0 : 0.27 : 8.6 : 30.0
$K^+\eta$	1	$-1.76 - i0.37$	$0.07 - i0.14$	$0.03 + i0.57$	$-1.67 + i0.06$	3.23 : 0.02 : 0.33 : 2.79
	2	$-1.18 - i0.52$	$0.03 - i0.09$	$0.10 + i0.58$	$-1.05 - i0.03$	1.66 : 0.01 : 0.35 : 1.10
$K^+\eta'$	1	$3.65 - i0.30$	$0.26 - i0.54$	$-0.41 - i2.99$	$3.50 - i3.83$	13.4 : 0.36 : 9.1 : 26.9
	2	$4.44 - i0.49$	$0.25 - i0.05$	$-0.38 - i3.07$	$4.31 - i4.08$	20.0 : 0.33 : 9.6 : 32.2

(i) For all the four considered decays, the factorizable emission diagrams Figs.1(a)-1(b) provide the dominant contribution to the branching ratios. In both MS-1 and MS-2 mixing schemes, we have

$$\frac{|\mathcal{M}^{c+d}|^2}{|\mathcal{M}^{a+b}|^2} < 0.01, \quad \frac{|\mathcal{M}^{anni}|^2}{|\mathcal{M}^{a+b}|^2} < 0.5, \tag{86}$$

for the two $B \to K\eta$ decays, and

$$\frac{|\mathcal{M}^{c+d}|^2}{|\mathcal{M}^{a+b}|^2} < 0.03, \quad \frac{|\mathcal{M}^{anni}|^2}{|\mathcal{M}^{a+b}|^2} < 0.7, \tag{87}$$

for the two $B \to K\eta'$ decays.

(ii) For all the four considered decays, one can see from Eqs.(86,87) that the contribution from the spectator diagrams Figs.1(c)-1(d) is very small in size,

$$\frac{|\mathcal{M}^{c+d}|^2}{|\mathcal{M}^{LO}|^2} < 0.03, \tag{88}$$

and therefore can be neglected safely, which is consistent with the general expectation. Since the LO part $\mathcal{M}^{c+d}$ is already negligibly small, it is reasonable for us to neglect the corresponding higher order NLO contribution $\mathcal{M}^{c+d}_{NLO}$ from the corresponding spectator diagrams Figs.5(a)-5(d).

(iii) For all the four considered decays, the real parts of $\mathcal{M}^{anni}$ are very small, but their imaginary parts are relatively large, this leads to a large strong phase, which is consistent with the general expectation. For the two $B \to K\eta'$ decays, the large imaginary parts of $\mathcal{M}^{anni}$ can also provide an effective enhancement to their branching ratios. From this point we understand that although the factorizable emission diagrams Figs.1(a)-1(b) provide the dominant contribution to the considered decays, but the LO contribution from the annihilation diagrams also provide essential contribution, therefore the NLO contribution $\mathcal{M}_{NLO}^{anni}$ from the corresponding annihilation diagrams as shown in Figs.5(e)-5(h) may be comparable with other NLO parts, and thus the analytical calculations for these diagrams should be done as soon as possible.

Now we study the relative strength for the NLO contributions from different sources and collect all numerical results in Table VIII and IX.

In Table VIII we list the numerical values for individual decay amplitudes. The decay amplitude $\mathcal{M}_{NLOWC}$ are obtained by evaluating the Figs.1(a)-1(h) with the use of the NLO Wilson coefficients $C_i(\mu)$, the NLO RG evolution matrix $U(t,m,\alpha)$ and $\alpha_s(\mu)$ at two-loop level. The label $\mathcal{M}_{VC}$ denotes the changes of $\mathcal{M}_{NLOWC}$ when only the NLO vertex corrections are included. The label $\mathcal{M}_{ql}$ ($\mathcal{M}_{mp}$) shows the changes of $\mathcal{M}_{NLOWC}$ when only the NLO contributions from the quark-loops (the chromo-magnetic penguin) are included. The label $\mathcal{M}_{FF}$ shows the variation of $\mathcal{M}_{NLOWC}$ when only the $B \to K$ and $B \to \eta^{(\prime)}$ transition form factors at NLO level are used.

The label $\mathcal{M}_{VC+ql+mp}$ and $\mathcal{M}_{NLO}$ in Table VIII and $\mathcal{M}_{NLO1}$ in Table IX are defined as the following summation:

$$\mathcal{M}_{VC+ql+mp} = \mathcal{M}_{VC} + \mathcal{M}_{ql} + \mathcal{M}_{mp}, \tag{89}$$

$$\mathcal{M}_{NLO1} = \mathcal{M}_{NLOWC} + \mathcal{M}_{VC+ql+mp}, \tag{90}$$

$$\mathcal{M}_{NLO}^{tot} = \mathcal{M}_{NLO1} + \mathcal{M}_{FF}. \tag{91}$$

Where $\mathcal{M}_{NLO1}$ is equivalent to the total decay amplitude $\mathcal{M}$ as defined in Eq.(76) of Ref. [12], and $\mathcal{M}_{NLO}$ is the decay amplitude when all currently known NLO contributions are taken into account.

The ratio R_{NLO} in Table IX is defined as

$$R_{NLO} = |\mathcal{M}_{LO}|^2 : |\mathcal{M}_{NLO1}|^2 : |\mathcal{M}_{NLO}^{tot}|^2. \tag{92}$$

TABLE VIII. The numerical values (in unit of 10^{-4}) of the individual NLO contributions to the decay amplitudes, coming from different sources in the η-η' and η-η'-G mixing scheme.

Decays	MS	$\mathcal{M}_{NLOWC}$	$\mathcal{M}_{VC}$	$\mathcal{M}_{ql}$	$\mathcal{M}_{mp}$	$\mathcal{M}_{VC+ql+mp}$	$\mathcal{M}_{FF}$
$K^0\eta$	1	$-1.54+i0.48$	$-0.03-i0.26$	$-0.32-i0.44$	$0.35-i0.27$	$-0.00-i0.97$	$0.05-i0.04$
	2	$-0.96+i0.54$	$-0.07-i0.08$	$-0.25-i0.36$	$0.22-i0.25$	$-0.10-i0.68$	$-0.001-i0.02$
$K^0\eta'$	1	$4.83-i3.94$	$0.63-i1.34$	$1.29+i1.59$	$-1.35+i0.37$	$0.57+i0.62$	$0.50-i0.25$
	2	$5.62-i4.03$	$0.61-i1.22$	$1.40+i1.73$	$-1.47+i0.36$	$0.54+i0.87$	$0.47-i0.24$
$K^+\eta$	1	$-1.65+i0.11$	$-0.05-i0.35$	$-0.32-i0.44$	$0.37-i0.27$	$0.00-i1.06$	$0.001-i0.18$
	2	$-1.13+i0.06$	$-0.10-i0.18$	$-0.25-i0.36$	$0.26-i0.26$	$-0.09-i0.80$	$-0.04-i0.13$
$K^+\eta'$	1	$4.66-i4.34$	$0.65-i1.38$	$1.30+i1.59$	$-1.38+i0.36$	$0.57+i0.57$	$0.46-i0.36$
	2	$5.39-i4.57$	$0.62-i1.29$	$1.41+i1.73$	$-1.50+i0.35$	$0.53+i0.79$	$0.43-i0.35$

From the numerical results as shown in Tables VII-IX, we find the following points:

TABLE IX. The numerical values of $\mathcal{M}_{LO}$, $\mathcal{M}_{NLO1}$, $\mathcal{M}_{NLO}$ (in unit of 10^{-4}) and the ratio R_{NLO} for $B \to K\eta^{(\prime)}$ decays in the η-η' and η-η'-G mixing schemes.

Decay	MS	$\mathcal{M}_{LO}$	$\mathcal{M}_{NLO1}$	$\mathcal{M}^{tot}_{NLO}$	R_{NLO}
$K^0\eta$	1	$-1.30+i0.47$	$-1.54-i0.49$	$-1.49-i0.53$	$1.91:2.61:2.50$
	2	$-0.76+i0.51$	$-1.05-i0.14$	$-1.05-i0.15$	$0.84:1.12:1.13$
$K^0\eta'$	1	$3.40-i3.29$	$5.41-i3.32$	$5.91-i3.57$	$22.4:40.3:46.3$
	2	$4.32-i3.37$	$6.16-i3.16$	$6.63-i3.40$	$30.0:47.9:55.5$
$K^+\eta$	1	$-1.67-i0.06$	$-1.65-i0.96$	$-1.65-i1.13$	$2.79:3.64:4.00$
	2	$-1.05-i0.03$	$-1.22-i0.74$	$-1.26-i0.87$	$1.10:2.04:2.35$
$K^+\eta'$	1	$3.50-i3.83$	$5.22-i3.77$	$5.69-i4.13$	$26.9:41.5:49.4$
	2	$4.31-i4.08$	$5.91-i3.78$	$6.34-i4.13$	$35.2:49.2:57.3$

(i) For all four $B \to K\eta^{(\prime)}$ decays, there are strong cancelation between $\mathcal{M}_{VC}$, $\mathcal{M}_{ql}$ and $\mathcal{M}_{mp}$.

(ii) For two $B \to K\eta$ decays, the corresponding $\mathcal{M}_{FF}$ are also much smaller in magnitude than other NLO parts $\mathcal{M}_{VC}$, $\mathcal{M}_{ql}$ and $\mathcal{M}_{mp}$, and also smaller in size than their summation $\mathcal{M}_{VC+ql+mp}$.

(iii) For two $B \to K\eta'$ decays, the corresponding $\mathcal{M}_{FF}$ are also much smaller than other NLO parts $\mathcal{M}_{VC}$, $\mathcal{M}_{ql}$ and $\mathcal{M}_{mp}$, but comparable in size with their summation $\mathcal{M}_{VC+ql+mp}$, and therefore all NLO contributions together provide the required enhancements to $Br(B \to K\eta')$ to account for the measured values.

(iv) The only missing NLO parts in the pQCD approach are $\mathcal{M}^{c+d}_{NLO}$ from Figs.5(a)-5(d) and $\mathcal{M}^{anni}_{NLO}$ from Figs.5(e)-5(h). They are most possibly small in size according to the studies in this paper and the general expectations based on the isospin cancelation and power suppression.

VI. SUMMARY

In this paper, we made a systematic study about the four $B \to K\eta^{(\prime)}$ decays in the pQCD factorization approach. We calculated the CP-averaged branching ratios and CP-violating asymmetries of the four $B \to K\eta^{(\prime)}$ decays in three different mixing schemes: the ordinary FKS η-η' mixing scheme, the η-η'-G and the η-η'-G-η_c mixing scheme. We considered the full LO contributions and all currently known NLO contributions to $B \to K\eta^{(\prime)}$ decays in the pQCD approach. Besides those NLO contributions considered in Ref. [12], we here also take the newly known NLO part of $B \to (K, \eta^{(\prime)})$ transition form factors into account.

From our numerical calculations and phenomenological analysis, we find the following points

(1) In all the three considered mixing schemes, the NLO pQCD predictions for the branching ratios and CP-violating asymmetries agree with the data within one stan-

dard deviation, of course, partially due to the still large theoretical errors. But the NLO pQCD predictions in the η-η'-G mixing scheme provide a nearly perfect interpretation for the measured values. The NLO pQCD predictions in MS-2 are the following:

$$\begin{aligned}
Br(B^0 \to K^0\eta) &= (1.13^{+1.95}_{-1.01}) \times 10^{-6}, \\
Br(B^0 \to K^0\eta') &= (66.5^{+25.9}_{-19.4}) \times 10^{-6}, \\
Br(B^\pm \to K^\pm\eta) &= (2.36^{+2.63}_{-1.50}) \times 10^{-6}, \\
Br(B^\pm \to K^\pm\eta') &= (67.3^{+26.0}_{-19.4}) \times 10^{-6},
\end{aligned} \tag{93}$$

for branching ratios, and

$$\begin{aligned}
\mathcal{A}^{dir}_{CP}(B^\pm \to K^\pm\eta) &= \left(-22.9^{+15.2}_{-19.1}\right) \times 10^{-2}, \\
\mathcal{A}^{dir}_{CP}(B^\pm \to K^\pm\eta') &= \left(-5.5^{+1.9}_{-1.9}\right) \times 10^{-2}, \\
\mathcal{A}^{dir}_{CP}(B^0 \to K^0_S\eta) &= \left(-16.0^{+7.9}_{-14.3}\right) \times 10^{-2}, \\
\mathcal{A}^{mix}_{CP}(B^0 \to K^0_S\eta) &= \left(66.7^{+3.7}_{-8.5}\right) \times 10^{-2}, \\
\mathcal{A}^{dir}_{CP}(B^0 \to K^0_S\eta') &= (3.3 \pm 0.3) \times 10^{-2}, \\
\mathcal{A}^{mix}_{CP}(B^0 \to K^0_S\eta') &= (70.0 \pm 0.3) \times 10^{-2},
\end{aligned} \tag{94}$$

for the CP-violating asymmetries, where the individual theoretical errors have been combined in quadrature.

(2) For $B^0 \to K^0\eta'$ and $B^+ \to K^+\eta'$ decays, the NLO contributions provide significant enhancements to their branching ratios. In the η-η'-G mixing scheme, for example, the NLO contribution provide a 89% (73%) enhancement to $Br(B^0 \to K^0\eta')$ ($Br(B^+ \to K^+\eta')$) with respect to the LO prediction, such enhancements play the key role in our effort to resolve the $K\eta^{(\prime)}$-puzzle and to understand the patten of the $Br(B \to K\eta^{(\prime)})$.

(3) For $B^0 \to K^0\eta$ and $B^+ \to K^+\eta$ decays, although the inclusion of the NLO contributions only leads to a relatively small changes to their branching ratios, but the resulted variations are in the right direction and helpful for us to improve the consistency between the pQCD predictions and the measured values. In the η-η'-G mixing scheme, for instance, the pQCD predictions are $Br(B^0 \to K^0\eta) = 0.90 \times 10^{-6}$ and $Br(B^+ \to K^+\eta) = 1.98 \times 10^{-6}$ at the leading order, and changed into $Br(B^0 \to K^0\eta) = 1.13 \times 10^{-6}$ and $Br(B^+ \to K^+\eta) = 2.36 \times 10^{-6}$ when the NLO contributions are taken into account, while the corresponding measured values are $1.23^{+0.27}_{-0.23} \times 10^{-6}$ and $2.36^{+0.22}_{-0.21} \times 10^{-6}$ respectively.

(4) By comparing the pQCD predictions as given in “NLO1” and “NLO” columns in Tables II-IV, one can see directly the effects of NLO form factors: the NLO part $\mathcal{M}_{FF}$ of the $B \to K$ and $B \to \eta^{(\prime)}$ form factors can produce about 20% enhancement to the branching ratios $Br(B \to K\eta')$, which plays an important role in closing the gap between the pQCD predictions and the relevant data.

(5) In the η-η'-G-η_c mixing scheme, the decay chain $B \to K\eta_c \to K\eta^{(\prime)}$ can provide an effective enhancement to the branching ratios at the leading-order. But when the large NLO contributions are taken into account, the effects of the η_c component become unimportant.

(6) For $B^\pm \to K^\pm\eta$ decays, the LO pQCD predictions for $\mathcal{A}_{CP}^{dir}$ in all three mixing schemes have an opposite sign with the measured value. The inclusion of the NLO contributions changed the sign of the pQCD predictions for $\mathcal{A}_{CP}^{dir}$, while the NLO pQCD predictions for $\mathcal{A}_{CP}^{dir}(B^\pm to K^\pm\eta)$ in the cases of MS-1 and MS-2 are now becoming consistent with the data within one standard deviation, but the NLO pQCD prediction for $\mathcal{A}_{CP}^{dir}(B^\pm \to K^\pm\eta)$ in the case of MS-3 is still much smaller than the measured value in magnitude.

(7) For $\mathcal{A}_{CP}^{dir}(B^\pm to K^\pm\eta')$, the NLO pQCD predictions agree with the data within one standard deviation, while the consistency between the pQCD predictions and the data are improved by the inclusion of the NLO contributions.

(8) For the direct and mixing-induced CP-violating asymmetries $\mathcal{A}_{CP}^{dir}(B^0 \to K_S^0\eta^{(\prime)})$ and $\mathcal{A}_{CP}^{mix}(B^0 \to K_S^0\eta^{(\prime)})$, the pQCD predictions have weak dependence on the NLO contributions and the choice of different mixing schemes. For $\mathcal{A}_{CP}^{dir,mix}(B^0 \to K_S^0\eta')$, for example, the NLO pQCD predictions are $\mathcal{A}_{CP}^{dir}(B^0 \to K_S^0\eta') \approx 3\%$ and $\mathcal{A}_{CP}^{mix}(B^0 \to K_S^0\eta') \approx 70\%$, which are well consistent with the measured values of $(1 \pm 9)\%$ and $(64 \pm 11)\%$ respectively.

(9) The factorizable emission diagrams Figs.1(a)-1(b) provide the dominant contribution to the considered decays. The LO contribution $\mathcal{M}^{c+d}$ from the spectator diagrams Figs.1(c)-1(d) is already less than 3% of the total contribution, the next-to-leading order contributions $\mathcal{M}_{NLO}^{c+d}$ from the diagrams Figs.5(a)-5(d) are the higher order contribution and therefore should be smaller than its LO counterpart. Consequently, it is reasonable for us to neglect $\mathcal{M}_{NLO}^{c+d}$ from the spectator diagrams Figs.5(a)-5(d).

(10) The real part of $\mathcal{M}^{anni}$ is always negligibly small, but its imaginary part is relatively large and leads to a large strong phase, which can also produce an effective enhancement to the branching ratios of the considered decays. Although $|\mathcal{M}_{NLO}^{anni}|$ is most possibly much smaller than its LO counterpart $|\mathcal{M}^{anni}|$, but the still missing NLO contribution $\mathcal{M}_{NLO}^{anni}$ from Figs.5(e)-5(h) may be comparable in size with $\mathcal{M}_{FF}$, and should be calculated as soon as possible.

ACKNOWLEDGMENTS

The authors are very grateful to Hsiang-nan Li, Cai-Dian Lu and Xin Liu for helpful discussions. This work is supported by the National Natural Science Foundation of China under the Grant No. 10975074 and 11235005; and by the Project on Graduate Students Education and Innovation of Jiangsu Province, under Grant No. CXLX11-0867;

Appendix A: Distribution Amplitudes

The expressions of the relevant distribution amplitudes (DA's) of K meson are the following [33]:

$$\phi_K^A(x) = \frac{f_K}{2\sqrt{2N_c}} 6x(1-x)\left[1 + a_1^K C_1^{3/2}(t) + a_2^K C_2^{3/2}(t) + a_4^K C_4^{3/2}(t)\right], \tag{A1}$$

$$\phi_K^P(x) = \frac{f_K}{2\sqrt{2N_c}} \left\{1 + (30\eta_3 - \frac{5}{2}\rho_K^2) C_2^{1/2}(t) - 3\left[\eta_3\omega_3 + \frac{9}{20}\rho_K^2(1+6a_2^K)\right] C_4^{1/2}(t)\right\}, \tag{A2}$$

$$\phi_K^T(x) = -\frac{f_K}{2\sqrt{2N_c}} t \left[1 + 6(5\eta_3 - \frac{1}{2}\eta_3\omega_3 - \frac{7}{20}\rho_K^2 - \frac{3}{5}\rho_K^2 a_2^K)(1 - 10x + 10x^2)\right], \tag{A3}$$

with the mass ratio $\rho_K = m_K/m_{0K}$. The Gegenbauer moments are of the form [33]:

$$a_1^K = 0.2, \quad a_2^K = 0.25, \quad a_4^K = -0.015. \tag{A4}$$

The values of other parameters are $\eta_3 = 0.015$ and $\omega = -3.0$. At last the Gegenbauer polynomials $C_n^\nu(t)$ are given as:

$$\begin{aligned}
&C_2^{1/2}(t) = \frac{1}{2}(3t^2 - 1), \quad C_4^{1/2}(t) = \frac{1}{8}(3 - 30t^2 + 35t^4),\\
&C_1^{3/2}(t) = 3t, \quad C_2^{3/2}(t) = \frac{3}{2}(5t^2 - 1),\\
&C_4^{3/2}(t) = \frac{15}{8}(1 - 14t^2 + 21t^4),
\end{aligned} \tag{A5}$$

with $t = 2x - 1$.

The distribution amplitudes $\phi_{\eta_q}^{A,P,T}$ are given as [33]:

$$\begin{aligned}
\phi_{\eta_q}^A(x) &= \frac{f_q}{2\sqrt{2N_c}} 6x(1-x)\left[1 + a_1^{\eta_q} C_1^{3/2}(2x-1) + a_2^{\eta_q} C_2^{3/2}(2x-1)\right.\\
&\quad \left. + a_4^{\eta_q} C_4^{3/2}(2x-1)\right],
\end{aligned} \tag{A6}$$

$$\begin{aligned}
\phi_{\eta_q}^P(x) &= \frac{f_q}{2\sqrt{2N_c}} \left[1 + (30\eta_3 - \frac{5}{2}\rho_{\eta_q}^2) C_2^{1/2}(2x-1)\right.\\
&\quad \left. -3\left\{\eta_3\omega_3 + \frac{9}{20}\rho_{\eta_q}^2(1 + 6a_2^{\eta_q})\right\} C_4^{1/2}(2x-1)\right],
\end{aligned} \tag{A7}$$

$$\begin{aligned}
\phi_{\eta_q}^T(x) &= \frac{f_q}{2\sqrt{2N_c}}(1-2x)\left[1 + 6\left(5\eta_3 - \frac{1}{2}\eta_3\omega_3 - \frac{7}{20}\rho_{\eta_q}^2 - \frac{3}{5}\rho_{\eta_q}^2 a_2^{\eta_q}\right)\right.\\
&\quad \left. \cdot \left(1 - 10x + 10x^2\right)\right],
\end{aligned} \tag{A8}$$

where $\rho_{\eta_q} = 2m_q/m_{qq}$,$a_1^{\eta_q} = a_1^\pi = 0$, $a_2^{\eta_q} = a_2^\pi = 0.44 \pm 0.22$, $a_4^{\eta_q} = a_4^\pi = 0.25$, and the Gegenbauer polynomials $C_n^\nu(t)$ have been given in Eq. (A5). As to the wave function and the corresponding DA's of the $s\bar{s}$ components, we also use the same form as $q\bar{q}$ but with some parameters changed: $\rho_{\eta_s} = 2m_s/m_{ss}$, $a_i^{\eta_s} = a_i^{\eta_q}$ for $i = 1, 2, 4$.

Appendix B: Related Hard Functions

In this appendix, we present the explicit expressions for those hard scales and hard functions.

The hard scales appeared in the decay amplitudes are chosen as

$$
\begin{aligned}
t_a &= \max\{\sqrt{x_3}M_B, 1/b_1, 1/b_3\},\\
t'_a &= \max\{\sqrt{x_1}M_B, 1/b_1, 1/b_3\},\\
t_b &= \max\{\sqrt{x_1x_3}M_B, \sqrt{|1-x_1-x_2|x_3}M_B, 1/b_1, 1/b_2\},\\
t'_b &= \max\{\sqrt{x_1x_3}M_B, \sqrt{|x_1-x_2|x_3}M_B, 1/b_1, 1/b_2\},\\
t_c &= \max\{\sqrt{1-x_3}M_B, 1/b_2, 1/b_3\},\\
t'_c &= \max\{\sqrt{x_2}M_B, 1/b_2, 1/b_3\},\\
t_d &= \max\{\sqrt{x_2(1-x_3)}M_B, \sqrt{1-(1-x_1-x_2)x_3}M_B, 1/b_1, 1/b_2\},\\
t'_d &= \max\{\sqrt{x_2(1-x_3)}M_B, \sqrt{|x_1-x_2|(1-x_3)}M_B, 1/b_1, 1/b_2\},\\
t_e &= \max\{\sqrt{x_3(1-r^2_{\eta_c})}M_B, 1/b_1, 1/b_3\},\\
t'_e &= \max\{\sqrt{x_1(1-r^2_{\eta_c})}M_B, 1/b_1, 1/b_3\},\\
t_f &= \max\{\sqrt{x_1x_3(1-r^2_{\eta_c})}M_B, \sqrt{|(-1+x_1+x_2)[x_3+(1-x_2-x_3)r^2_{\eta_c}]+r^2_{\eta_c}|}M_B,\\
&\quad 1/b_1, 1/b_2\},\\
t'_f &= \max\{\sqrt{x_1x_3(1-r^2_{\eta_c})}M_B, \sqrt{|(x_1-x_2)[x_3+(x_2-x_3)r^2_{\eta_c}]+r^2_{\eta_c}|}M_B,\\
&\quad 1/b_1, 1/b_2\}.
\end{aligned}
\tag{B1}
$$

The hard functions h_is appeared in the decay amplitudes are defined by

$$
\begin{aligned}
h_e(x_1,x_3,b_1,b_3) &= [\theta(b_1-b_3)I_0(\sqrt{x_3}M_Bb_3)K_0(\sqrt{x_3}M_Bb_1)\\
&\quad +\theta(b_3-b_1)I_0(\sqrt{x_3}M_Bb_1)K_0(\sqrt{x_3}M_Bb_3)]\,K_0(\sqrt{x_1x_3}M_Bb_1)S_t(x_3),\\
h_n(x_1,x_2,x_3,b_1,b_2) &= [\theta(b_2-b_1)K_0(\sqrt{x_1x_3}M_Bb_2)I_0(\sqrt{x_1x_3}M_Bb_1)\\
&\quad +\theta(b_1-b_2)K_0(\sqrt{x_1x_3}M_Bb_1)I_0(\sqrt{x_1x_3}M_Bb_2)]\\
&\quad \times\left\{\begin{array}{ll} \frac{i\pi}{2}H_0^{(1)}(\sqrt{(x_2-x_1)x_3}M_Bb_2), & x_1-x_2<0\\ K_0(\sqrt{(x_1-x_2)x_3}M_Bb_2), & x_1-x_2>0 \end{array}\right.,
\end{aligned}
\tag{B2}
$$

$$
\begin{aligned}
h_a(x_2,x_3,b_2,b_3) &= (\frac{i\pi}{2})^2S_t(x_3)\Big[\theta(b_2-b_3)H_0^{(1)}(\sqrt{x_3}M_Bb_2)J_0(\sqrt{x_3}M_Bb_3)\\
&\quad +\theta(b_3-b_2)H_0^{(1)}(\sqrt{x_3}M_Bb_3)J_0(\sqrt{x_3}M_Bb_2)\Big]\,H_0^{(1)}(\sqrt{x_2x_3}M_Bb_2),\\
h_{na}(x_1,x_2,x_3,b_1,b_2) &= \frac{i\pi}{2}\,\Big[\theta(b_1-b_2)H_0^{(1)}(\sqrt{x_2(1-x_3)}M_Bb_1)J_0(\sqrt{x_2(1-x_3)}M_Bb_2)\\
&\quad +\theta(b_2-b_1)H_0^{(1)}(\sqrt{x_2(1-x_3)}M_Bb_2)J_0(\sqrt{x_2(1-x_3)}M_Bb_1)\Big]\\
&\quad \times K_0(\sqrt{1-(1-x_1-x_2)x_3}M_Bb_1),
\end{aligned}
\tag{B3}
$$

$$\begin{aligned} h'_{na}(x_1,x_2,x_3,b_1,b_2) = \frac{i\pi}{2}\Big[&\theta(b_1-b_2)H_0^{(1)}(\sqrt{x_2(1-x_3)}M_Bb_1)J_0(\sqrt{x_2(1-x_3)}M_Bb_2) \\ &+\theta(b_2-b_1)H_0^{(1)}(\sqrt{x_2(1-x_3)}M_Bb_2)J_0(\sqrt{x_2(1-x_3)}M_Bb_1)\Big] \\ &\times\left\{\begin{array}{ll} \frac{i\pi}{2}H_0^{(1)}(\sqrt{(x_2-x_1)(1-x_3)}M_Bb_1), & x_1-x_2<0 \\ K_0(\sqrt{(x_1-x_2)(1-x_3)}M_Bb_1), & x_1-x_2>0 \end{array}\right. , \end{aligned} \tag{B4}$$

where $H_0^{(1)}(z) = \mathrm{J}_0(z) + i\,\mathrm{Y}_0(z)$.

$$\begin{aligned} h'_e(x_1,x_3,b_1,b_3) = \big[&\theta(b_1-b_3)I_0(\sqrt{\alpha}M_Bb_3)K_0(\sqrt{\alpha}M_Bb_1) \\ &+\theta(b_3-b_1)I_0(\sqrt{\alpha}M_Bb_1)K_0(\sqrt{\alpha}M_Bb_3)\big]\,K_0(\sqrt{\beta}M_Bb_1)S_t(x_3), \end{aligned} \tag{B5}$$

where $\alpha = x_3(1-r_{\eta_c}^2)$, $\beta = x_1x_3(1-r_{\eta_c}^2)$.

$$\begin{aligned} h'_n(x_1,x_2,x_3,b_1,b_2) = \Big[&\theta(b_2-b_1)K_0(\sqrt{\alpha'}M_Bb_2)I_0(\sqrt{\alpha'}M_Bb_1) \\ &+\theta(b_1-b_2)K_0(\sqrt{\alpha'}M_Bb_1)I_0(\sqrt{\alpha'}M_Bb_2)\Big] \\ &\times\left\{\begin{array}{ll} \frac{i\pi}{2}H_0^{(1)}(\sqrt{|\beta'^2|}M_Bb_2), & \beta'^2<0 \\ K_0(\sqrt{|\beta'^2|}M_Bb_2), & \beta'^2>0 \end{array}\right. , \end{aligned} \tag{B6}$$

where $\alpha' = x_1x_3(1-r_{\eta_c}^2)$, $\beta'^2 = (x_1-x_2)[x_2r_{\eta_c}^2 + x_3(1-r_{\eta_c}^2)] + r_{\eta_c}^2$.

The function $S_t(x)$ has been parameterized as [34]

$$S_t(x) = \frac{2^{1+2c}\Gamma(3/2+c)}{\sqrt{\pi}\Gamma(1+c)}[x(1-x)]^c, \tag{B7}$$

with $c = 0.3$.

The evolution factors $E_e^{(\prime)}$, and $E_a^{(\prime)}$, appeared in the decay amplitudes are given by

$$\begin{aligned} E_e(t) &= \alpha_s(t)\exp[-S_B(t)-S_3(t)], \\ E'_e(t) &= \alpha_s(t)\exp[-S_B(t)-S_2(t)-S_3(t)]|_{b_1=b_3}, \\ E_a(t) &= \alpha_s(t)\exp[-S_2(t)-S_3(t)], \\ E'_a(t) &= \alpha_s(t)\exp[-S_B(t)-S_2(t)-S_3(t)]|_{b_2=b_3}, \end{aligned} \tag{B8}$$

where the Sudakov exponents are defined as

$$\begin{aligned} S_B(t) &= s\left(x_1\frac{M_B}{\sqrt{2}}, b_1\right) + \frac{5}{3}\int_{1/b_1}^{t}\frac{d\bar{\mu}}{\bar{\mu}}\gamma_q(\alpha_s(\bar{\mu})), \\ S_2(t) &= s\left(x_2\frac{M_B}{\sqrt{2}}, b_2\right) + s\left((1-x_2)\frac{M_B}{\sqrt{2}}, b_2\right) + 2\int_{1/b_2}^{t}\frac{d\bar{\mu}}{\bar{\mu}}\gamma_q(\alpha_s(\bar{\mu})), \end{aligned} \tag{B9}$$

with the quark anomalous dimension $\gamma_q = -\alpha_s/\pi$. Replacing the kinematic variables of M_2 to M_3 in S_2, we can get the expression for S_3. The explicit form for the functions $s(Q,b)$ can be found in Ref. [21].

---

[1] B.H. Behrens, CLEO Collaboration, Phys. Rev. Lett. **80**, 3710 (1998).

[2] A.L. Kagan and A.A. Petrov, hep-ph/9707354; S. Khalil and E. Kou, Phys. Rev. Lett. **91**, 241602 (2003).

[3] G.R. Lu, Z.J. Xiao, H.K. Guo and L.X. Lü, J. Phys. G **25**, L85 (1999); Z.J. Xiao, K.T. Chao and C.S. Li, Phys. Rev. D **65**, 114021(2002); Z.J. Xiao and W.J. Zou, Phys. Rev. D **70**, 094008 (2004).

[4] M.Z. Yang and Y.D. Yang, Nucl. Phys. B **609**, 469 (2001).

[5] Y.-Y. Keum, H.N. Li and A.I. Sanda, Phys. Rev. D **63**, 054008 (2001).

[6] C.D. Lü, K. Ukai and M.Z. Yang, Phys. Rev. D **63**, 074009 (2001).

[7] M. Beneke and M. Neubert, Nucl. Phys. B **651**, 225 (2003).

[8] E. Kou and A. Sanda, Phys. Lett. B **525**, 240 (2002).

[9] H.N. Li, Prog. Part. & Nucl. Phys. **51**, 85 (2003) and references therein.

[10] Y. Amhis *et al.*, (Heavy Flavor Averaging Group), arXiv:1207.1158 [hep-ex] and online update at http://www.slac.stanford.edu/xorg/hfag.

[11] J. Beringer *et al.* (Particle Data Group), Phys. Rev. D **86**, 010001 (2012).

[12] Z.J. Xiao, Z.Q. Zhang, X. Liu, and L.B. Guo, Phys. Rev. D **78**, 114001 (2008).

[13] Th. Feldmann, P. Kroll, and B. Stech, Phys. Rev. D **58**, 114006 (1998); Phys. Lett. B **449**, 339 (1999).

[14] H.N. Li, Y.L. Shen, and Y.M. Wang, Phys. Rev. D **85**, 074004 (2012).

[15] X. Liu, H.N. Li, and Z.J. Xiao, Phys. Rev. D **86**, 011501(R)(2012).

[16] H.Y. Cheng, H.N. Li, and K.F. Liu, Phys. Rev. D **79**, 014024 (2009).

[17] Y.Y. Charng, T. Kurimoto, and H.N. Li, Phys. Rev. D **74**, 074024 (2006); **78**, 059901(E) (2008).

[18] Y.D. Tsai, H.N. Li, and Qiang Zhao, Phys. Rev. D **85**, 034002 (2012).

[19] X. Liu, H.S. Wang, Z.J. Xiao, L.B. Guo, and C.D. Lü, Phys. Rev. D **73**, 074002 (2006); H.S. Wang, X. Liu, Z.J. Xiao, L.B. Guo, and C.D. Lü, Nucl. Phys. B **738**, 243 (2006); Z.J. Xiao, D.Q. Guo, and X.F. Chen, Phys. Rev. D **75**, 014018 (2007); D.Q. Guo, X.F. Chen, and Z.J. Xiao, Phys. Rev. D **75**, 054033 (2007); X.F. Chen, D.Q. Guo, and Z.J. Xiao, Eur. Phys. J. C **50**, 363 (2007).

[20] A. Ali, G. Kramer, Y. Li, C.D. Lü, Y.L. Shen, W. Wang, and Y.M. Wang, Phys. Rev. D **76**, 074018 (2007).

[21] H.N. Li, S. Mishima, A.I. Sanda, Phys. Rev. D **72**, 114005 (2005), and referrences therein.

[22] H.Y Cheng, K.C Yang, Phys. Rev. D **63**, 074011 (2001).

[23] X. Liu, Z.Q. Zhang, Z.J. Xiao, Chin. Phys. C **34**, 937 (2010).

[24] X. Liu, Z.J. Xiao, and C.D. Lu, Phys. Rev. D **81**,014022(2010); X. Liu and Z.J. Xiao, Phys. Rev. D **81**, 074017 (2010); Phys. Rev. D **82**, 054029(2010); J. Phys. G **38**, 035009 (2011); Z.J. Xiao and X. Liu, Phys. Rev. D **84**, 074033 (2011).

[25] Z.J. Xiao, W.F. Wang, and Y.Y. Fan, Phys. Rev. D **85**, 094003 (2012).

[26] Y. Li, C.D. Lü, Z.J. Xiao, and X.Q. Yu, Phys. Rev. D **70**, 034009 (2004).

[27] H.N. Li, Y.L. Shen, Y.M. Wang, and H. Zou, Phys. Rev. D **83**, 054029 (2011).

[28] G. Buchalla, A.J. Buras, and M.E. Lautenbacher, Rev. Mod. Phys.**68**, 1125 (1996).

[29] A.E. Bondar, V.L. Chernyak, Phys. Lett. B **612**, 215 (2005).

[30] M. Beneke, G. Buchalla, M. Neubert, and C.T. Sachrajda, Phys. Rev. Lett. **83**, 1914 (1999); Nucl. Phys. B **591**, 313 (2000).

[31] M. Beneke and M. Neubert, Nucl. Phys. B **675**, 333 (2003).

[32] S. Mishima and A.I. Sanda, Prog. Theor. Phys. **110**, 549 (2003).

[33] P. Ball, V.M. Braun, Y. Koike, and K. Tanaka, Nucl. Phys. B **529**, 323 (1998); P. Ball, J. High Energy Phys. 9809 (1998) 005; J. High Energy Phys. 9901 (1999) 010; P. Ball and R. Zwicky, Phys. Rev. D **71**, 014015 (2005); J. High Energy Phys. 0604 (2006) 046.

[34] T. Kurimoto, H.N. Li, and A.I. Sanda, Phys. Rev. D **65**, 014007 (2001); H.N. Li, Phys. Rev. D **66**, 094010 (2002).